Discriminant Model for Cytologic Distinction of Large Cell Neuroendocrine Carcinoma from Small Cell Carcinoma of the Lung

Rira Hoshi, CT, Noriyuki Furuta, CT,* Takeshi Horai, MD,* Yuichi Ishikawa, MD, PhD,† Satoshi Miyata, PhD,‡ and Yukitoshi Satoh, MD, PhD*§*

Background: To establish cytologic criteria for pulmonary large cell neuroendocrine carcinoma (LCNEC), we developed and evaluated a discriminant model for cytologic differential diagnosis between LCNEC and small cell lung carcinoma (SCLC).

Methods: Aspiration cytologic and/or imprint smears from 29 LCNEC cases were reviewed in comparison with 26 SCLC cases. We selected the following parameters for assessment: background, cellular arrangement, cell clusters, cell cohesion, arrangements, cell dimensions areas, the presence of cytoplasm and/or prominent nucleoli, nuclear features, mitosis, naked nuclei, and nuclear streaking. To demonstrate the utility of differences in frequencies of cytologic parameters for LCNECs and SCLCs, a discriminant model was developed and evaluated.

Results: Among the cytologic parameters investigated, large clusters (consisting of $\geq$60 tumor cells) with tight cohesion and small tumor cells (showing $\leq$120 μm^2) without prominent nucleoli on each case were particular focuses of attention, because statistically significant differences with good power were evident between the LCNEC and SCLC groups for their frequencies ($p < 0.0001$). On the basis of variation in plotted location on scatter plots, a discriminant model for LCNEC and SCLC was made and evaluated by logistic discriminant analysis. Sensitivity, specificity, and accuracy were all 100%. With leave-one-out cross validation, the predicted error rate of the discriminant model for new cases was 0.00545.

Conclusion: Our model based on the cytologic features of large cell clusters with tight cohesion and of small tumor cells without prominent nucleoli should be a useful aid for distinction between LCNECs and SCLCs.

From the *Departments of Cytology, Cancer Institute Hospital, Japanese Foundation of Cancer Research, Tokyo, Japan; †Department of Pathology, and ‡Bioinformatics Group, Genome Center, the Cancer Institute, the Japanese Foundation for Cancer Research, Tokyo, Japan; and §Department of Thoracic Surgery, Kitasato University School of Medicine, Kanagawa, Japan.

Disclosure: The authors declare no conflicts of interest.

Address for correspondence: Yukitoshi Satoh, MD, PhD, Department of Thoracic Surgery, Kitasato University School of Medicine, 1-15-1 Kitasato, Sagamihara-shi, Kanagawa 228-8555, Japan. Email: ysatoh@med.kitasato-u.ac.jp

Copyright © 2010 by the International Association for the Study of Lung Cancer

ISSN: 1556-0864/10/0504-0472

Key Words: Lung cancer, Large cell neuroendocrine carcinoma, Small cell lung carcinoma, Discriminant model, Cytology.

(*J Thorac Oncol.* 2010;5: 472–478)

Large cell neuroendocrine carcinoma (LCNEC) of the lung and small cell lung carcinoma (SCLC) are both now considered as high-grade neuroendocrine carcinomas arising in the lung.[1–4] Based on the large, multiinstitutional study in Japan, Asamura et al.[5] reported that the 5-year survival rates of patients with all stages were 40.3% for LCNEC and 35.7% for SCLC, the differenc not being statistically significant. However, these two tumors are generally thought to have different clinical features[1,4,6–14] and require different treatments.

Currently, surgical resection is advocated for the LCNEC as same as other nonsmall cell lung cancers.[15] However, Iyoda et al.[10] reported that patients with stage I disease treated with either neoadjuvant or postoperative adjuvant chemotherapy had a significantly better prognosis than their counterparts groups receiving surgery alone. Therefore, LCNEC requires a refined histology-specific approach. Conversely, the SCLC is aggressive but chemosensitive, and a standard therapeutic strategy has already been established.[5]

The cytologic diagnosis of SCLC is clear, but criteria for the LCNEC have yet to be established.[5,16–22] Recently, the cytologic features of LCNEC described in several reports are as follows: necrotic background, loose cell aggregates, large cell size (three times as large as mature lymphocytes), rosette and Indian-filing arrangements, abundant cytoplasm, granular nuclear chromatin, clear nucleoli, naked nuclei, and nuclear streaking.[17–22] Because these are also often recognized in SCLC cases,[15,16,23] they are not specific.

The aim of this study was to elucidate the cytologic characteristics of the LCNEC in comparison with SCLCs particularly and evaluate the utility of proposed scoring system for their differential diagnosis.

MATERIALS AND METHODS

Patients

The pathology files of the Cancer Institute Hospital (Tokyo, Japan) between 1990 and 2007 were searched for 29 patients who underwent pulmonary resection for LCNECs.

These LCNEC cases were all confirmed by pathologic examination on surgically resected materials with the World Health Organization (WHO) classification system.[15] The histologic diagnostic criteria of LCNEC proposed by WHO are as follows: neuroendocrine morphologic features (organoid nesting, palisading, rosettes, and trabecular growth pattern); a high mitotic rate (>10 per 10 high-power fields); necrosis (often large zones); cellular features of a nonsmall cell carcinoma (large cell size, a low nuclear/cytoplasmic ratio, polygonal shape, finely granular eosinophilic cytoplasm, coarse chromatin, and/or frequent nucleoli); and neuroendocrine features by immunohistochemistry or electron microscopy or both.[15] For comparison, we randomly extracted 26 cases of SCLCs diagnosed during the same period, 16 of which were diagnosed with surgical materials and the remaining 10 with transbronchial lung biopsy samples. The histologic diagnosis of SCLCs was also based on the WHO classification system.[15] Combined LCNECs and SCLCs and SCLC cases after any treatment were all excluded in this study, which was approved by our institutional review board, each patient giving written informed consent before treatment.

Cytologic Materials

Cytologic specimens obtained by transbronchial aspiration and/or imprint from the resected specimens were fixed routinely in 95% ethanol and stained by the Papanicolaou method. Five to 12 cytologic slides were reviewed for each patient. From previous studies,[17–22] we selected the following parameters for assessment: necrotic background, cellular arrangement, tumor cell clusters, tumor cell cohesion, cell arrangements, cell dimensions areas, the presence of tumor cells with identifiable cytoplasm and/or prominent nucleoli, nuclear features, mitosis, naked nuclei, and nuclear streaking. Cluster size was categorized in the three groups as follows: small clusters, consisting of more than 10 and less than or equal to 20 cells; intermediate-sized clusters, consisting of more than 20 cells and less than 60 cells; and large clusters, consisting of more than or equal to 60 cells. Tight cohesiveness of clusters was defined as a straight cluster border composed of cells lined up and/or arranged in palisades. Cell areas were measured for 50 cells extracted at random in each specimen and calculated as (long diameter + short diameter/$2 \times 2)^2 \pi$ ($\pi = 3.14$). The diameters of tumor cells were measured using an ocular micrometer (DSM; Olympus, Tokyo, Japan). Cell size was categorized in 2 groups as follows: small tumor cells, less than or equal to 120 μm^2; and large tumor cells, more than or equal to 600 μm^2.

Statistical Analysis

The clinicopathologic factors analyzed in this study included age (<65 or ≥65 years), gender, and smoking habits, evaluated by the χ^2 test. Differences in cell areas and the frequency of the cytologic features between LCNEC and SCLC cases were analyzed by an unpaired Student t test and χ^2 test; $p < 0.05$ was considered significant.

Logistic Discriminant Analysis

To demonstrate the utility of differences in frequencies of cytologic parameters for LCNECs and SCLCs, a discriminant model was developed and evaluated. The frequencies of two cytologic features, in which differences were statistically significant, were regarded as two variables for a set of data, displayed as a scatter plot. By logistic discriminant analysis based on the scatter plots, a discriminant model for LCNEC and SCLC was made. When two variables for frequency of cytologic features were regarded as x_1 and x_2, the probability of an SCLC was calculated as follows.

$$P(SCLC) = \frac{\exp(-319.81 - 10.82x_1 + 16.30x_2)}{1 + \exp(-319.81 - 10.82x_1 + 16.30x_2)}$$

And the discriminant line was as follows.

$$-319.81 - 10.82x_1 + 16.30x_2 = 0 \Leftrightarrow x_2 = 19.62 + 0.6641x_1$$

We regarded a point on upper part of the line as true (SCLCs) and a point on lower part of the line as false (LCNECs). Furthermore, we analyzed prediction of error discrimination for new cases by leave-one-out cross validation. A discriminant model for LCNEC and SCLC was made except in one case. The excepted case was predicted by the discriminant model, and the discrimination confirmed whether it was correct. For all SCLC and LCNEC cases, the same analyses were performed repeatedly.

RESULTS

Clinical Findings

Clinicopathologic findings for the 29 LCNEC patients are summarized in Table 1. There were 26 men and 3 women, ranging in age from 48 to 80 years, with a median of 67 years. Lobectomy was performed on all. Mean follow-up time was 2.4 years (range, 0.33–9 years); 14 were dead, and 15 were alive at the time of this analysis. All patients had a smoking habit, ranging from 3 to 206.5 pack years. Of the 26 SCLC patients, 19 were men and 7 women, ranging in age from 58 to 80 years, with a median of 69 years. Eight were treated with surgical resection and eight with surgical resection after chemotherapy. In these 16 cases, no combination of SCLC with other histologic types was identified on resected materials. The remaining 10 underwent chemotherapy and/or radiotherapy, but again no admixture of other types was noted in biopsy specimens. Mean follow-up for the 26 patients was 2.6 years (range, 0.08–8 years); 14 were dead, and 12 were alive at the time of this analysis. All patients also had a smoking habit. A comparison of data for LCNEC and SCLC groups revealed no statistically significant differences in age, gender, and smoking status (Table 1).

Cytologic Findings

The initial cytologic diagnoses of 29 LCNEC patients were 4 LCNECs, 5 SCLCs, 2 combined SCLCs and adenocarcinomas, 5 neuroendocrine carcinomas, 1 atypical carcinoid, 7 poorly differentiated adenocarcinomas, 3 poorly differentiated squamous cell carcinomas, and 2 nonsmall cell carcinomas. In the LCNEC group, the unanimity in diagnosis between pathology and cytology was 21.1%. The cytologic

Copyright © 2010 by the International Association for the Study of Lung Cancer

TABLE 1. Clinicopathologic Findings for LCNEC and SCLC Cases

Characteristic	No. of Patients	LCNEC (n = 29)	SCLC (n = 26)	p
Age (yr)				
<65	14	9	5	0.32
≤65	41	20	21	
Gender				
Male	45	26	19	0.11
Female	10	3	7	
Smoking status				
Nonsmoker	0	0	0	1.00
Smoker	55	29	26	
Cytologic materials				
TBAC	34	16	18	0.56
IC	5	3	2	
TBAC and IC	16	10	6	
Cytologic diagnosis				
LCNEC	4	4	0	<0.0001
LCNEC > SCLC	2	2	0	
NE	4	4	0	
SCLC	31	5	26	
SCLC + NSCLC	2	2	0	
NSCLC	12	12	0	
Tumor location				
Right lung	5	—	5	—
RUL	15	12	3	
RLL	12	7	5	
Left lung	2	—	2	
LUL	14	9	5	
LLL	7	1	6	
Type of location				
Central	11	3	8	0.09
Peripheral	44	26	18	
Tumor size (cm)				
≤3.0	25	12	13	—
>3.0	24	17	7	
NA	6	0	6	
Pathologic stage (pTNM)				
IA	14	8	6	—
IB	12	11	1	
IIA	5	1	4	
IIB	4	3	1	
IIIA	8	4	4	
IIIB	2	1	1	
IV	6	1	5	
NA(LD)	4	—	4	
Survival after surgery				
Dead	28	14	14	0.68
Alive	27	15	12	
Mean ± SD		2.39 ± 2.27	2.63 ± 2.33	

TBAC, transbronchial aspiration cytology; IC, imprint cytology; LCNEC, large cell neuroendocrine carcinoma; SCLC, small cell lung carcinoma; NE, neuroendocrine carcinoma; NSLC, nonsmall cell lung carcinoma; RUL, right upper lobe; RLL, right lower lobe; LUL, left upper lobe; LLL, left lower lobe; NA, not available; pTNM, from Ref. 15; LD, Limited disease.

TABLE 2 Cytologic Comparison Between LCNEC and SCLC

Cytologic Parameters	LCNEC (n = 29)	SCLC (n = 26)	p value
Necrotic background	25/29 (86.2%)	23/26 (88.5%)	0.802
Predominant cellular arrangement			
Cluster	26/29 (89.7%)	5/26 (19.2%)	
Single cells	3/29 (10.3%)	21/26 (80.7%)	<0.0001
Presence of characteristic clusters			
Large sized	27/29 (93.1%)	4/26 (15.4%)	<0.0001
Strong cohesion	27/29 (93.1%)	3/26 (11.5%)	<0.0001
Presence of tumor cell arrangement			
Rosette	28/29 (96.6%)	21/26 (80.7%)	0.061
Molding	26/29 (89.7%)	26/26 (100 %)	0.092
Pair cells	12/29 (41.3%)	17/26 (65.4%)	0.075
Palisading	27/29 (93.1%)	3/26 (11.5%)	<0.0001
Mean tumor cell size	178.1 μm^2	127.2 μm^2	<0.0001
Presence of characteristic tumor cells			
Large sized	18/29 (62.0%)	20/26 (76.9%)	0.224
Evidently identifiable cytoplasm	27/29 (93.1%)	20/26 (76.9%)	0.089
Prominent nucleoli	24/29 (82.8%)	20/26 (76.9%)	0.589
Small sized without prominent nucleoli	15/29 (51.7%)	26/26 (100 %)	<0.0001
Chromation pattern			
Finely granular	10/29 (34.5%)	11/26 (42.3%)	
Finely granular to granular	14/29 (48.3%)	15/26 (57.7%)	0.085
Granular	5/29 (17.2%)	0/26 (0 %)	
Presence of characteristics			
Mitoses	25/29 (86.2%)	25/26 (96.2%)	0.200
Nuclear streaking	26/29 (89.7%)	25/26 (96.2%)	0.354
Naked nuclei	24/29 (82.8%)	10/26 (38.5%)	0.0007

diagnoses for the 26 SCLC patients were all SCLCs, with statistically significant unanimity ($p < 0.0001$).

In a preliminary study, we evaluated any cytologic differences between aspiration smears and touch preparations in pilot groups consisting of 10 cases each of LCNEC and SCLC. In these groups, aspiration preparations and imprints showed no significant differences in any of the parameters chosen for assessment (data not shown). Comparisons between LCNEC and SCLC for each cytologic parameter are shown in Table 2. Cytologic parameters with statistically significant differences were as follows: cellular arrangement, presence of large clusters, tumor cell cohesion, palisading arrangement of tumor cells, mean of cellular areas, and presence of small cells without prominent nucleoli and naked nuclei. With regard to cellular arrangement, single cells were evident in all SCLC cases, whereas tumor cell clusters were frequently observed in LCNECs (Figures 1, 2). In the LCNEC group, although single cells were evident, many of them had naked nuclei. In particular, large clusters consisting of more than 60 cells were characteristic in LCNEC group

Copyright © 2010 by the International Association for the Study of Lung Cancer

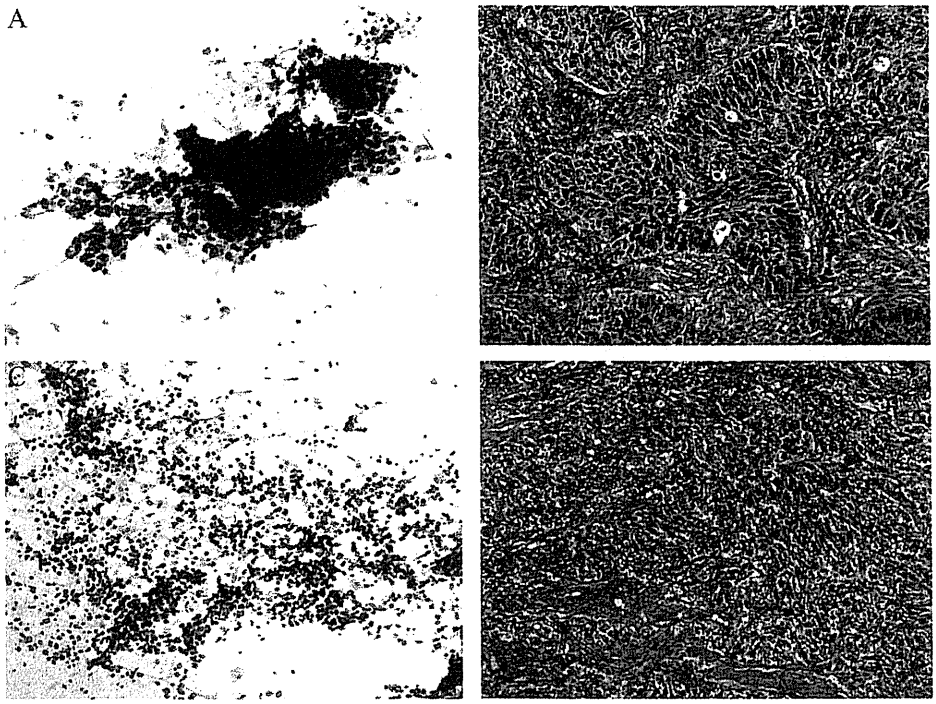

FIGURE 1. Photomicrographs illustrating cellular arrangement in transbronchial aspiration or histology specimens of LCNEC and SCLC cases. *A*, Large and three-dimensional clusters are conspicuous in a cytologic smear of an LCNEC case (Papanicolaou stain, ×20); *B*, tumor nests of an LCNEC case show palisading and Rosette-like formations in a histology specimen (hematoxylin and eosin stain, ×40); *C*, single cells are conspicuous in the cytologic smear of an SCLC case (Papanicolaou stain, ×20); and *D*, tumor cells of an SCLC case comprise irregular nests in a histology specimen (hematoxylin and eosin stain, ×40).

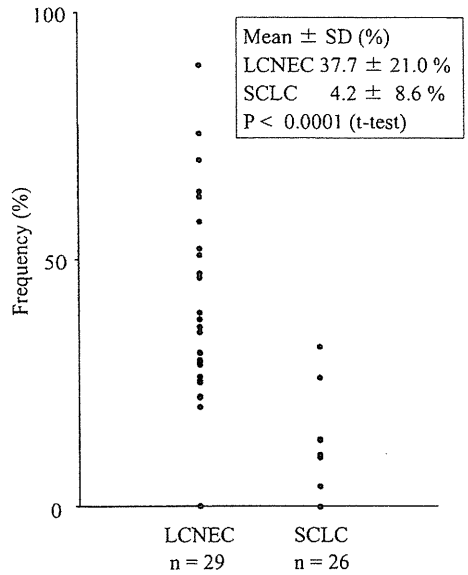

FIGURE 2. Frequencies of large clusters with tight cohesion in the LCNEC and SCLC groups (n = 55).

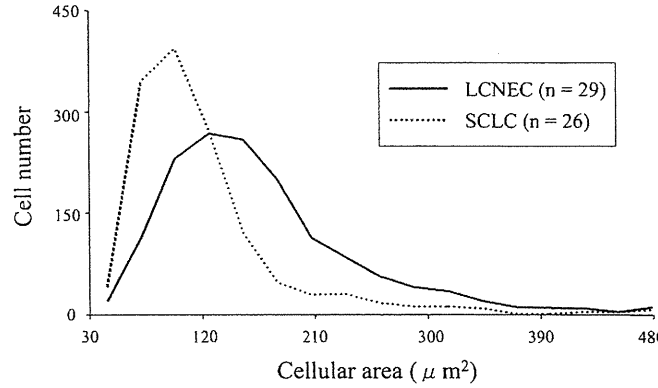

FIGURE 3. Histograms of cell areas in LCNEC and SCLC groups. Note that about 60% of the SCLC cells fall in the range of less than 120 μm^2, as compared with about 25% for LCNEC cells ($p < 0.0001$).

(Figures 1, 2). Also, on those histologic specimens, cell adhesion between tumor cells of LCNEC cases was conspicuous, whereas it was indistinct in SCLC cases (Figures 1*B*, *D*).

Furthermore, tumor cell cohesion was weak in SCLC cases, whereas in LCNEC cases tightly cohesive clusters predominated (Table 2). Frequencies of large clusters with tight cohesion are shown in Figure 3. The mean frequency was 37.7 ± 21.0% in the LCNEC cases and 4.2 ± 8.4% in SCLCs, the difference being statistically significant ($p < 0.0001$). LCNEC cases featured discrete cell nests divided by fibrous stroma with frequent peripheral palisading, whereas SCLC cases were characterized by cell nests, frequently infiltrating adjacent fibrous stroma (Figure 1).

Mean cell areas were 178.1 ± 84.8 μm^2 (range, 45.3–808.9 μm^2) for LCNEC cases and 127.8 ± 69.3 μm^2 (range, 36.8–699.5 μm^2) for SCLCs, the difference being statistically significant ($p < 0.0001$). The distributions are shown graphically in Figure 3. Some 58.2% of the SCLC cells (756/1300) were less than 120 μm^2, as compared with only 24.6% for LCNEC cells (357/1450; $p < 0.0001$). Furthermore, small tumor cells lacking prominent nucleoli in SCLC cases were observed more frequently than in LCNEC cases ($p < 0.0001$; Table 2 and Figure 5). Frequencies are shown in Figure 4. The mean values were 11.9 ± 12.1% in LCNEC and 55.8 ± 18.9% in SCLC cases, the difference being

Copyright © 2010 by the International Association for the Study of Lung Cancer

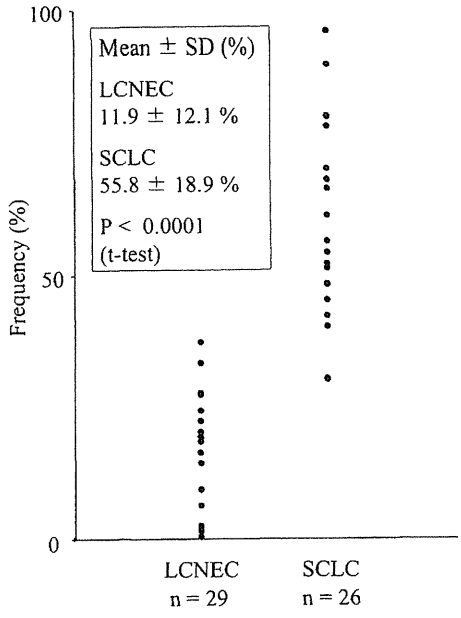

FIGURE 4. Frequencies of small tumor cells without prominent nucleoli in the LCNEC and SCLC groups (n = 55).

statistically significant ($p < 0.0001$). Also, in histologic specimens, SCLC cases had the cell nests predominantly composed of small tumor cells with scant cytoplasm without nucleoli, whereas LCNEC cases demonstrated cell nests predominantly composed of large tumor cells with abundant cytoplasm and occasional prominent nucleoli (Figure 5*B*, *D*).

Logistic Discriminant Analysis

For the frequencies of large clusters with tight cohesion and small tumor cells without prominent nucleoli, statistically significant differences with strong power was evident between LCNEC and SCLC groups. Therefore, these two cytologic parameters were considered as the two variables for the scatter plots. The dots for LCNEC cases are located on the lower right, whereas those of SCLC cases were located on the upper left, with clear differences between the two for the majority. The results of logistic discriminant analysis are shown in Figure 6. Because all SCLC and LCNEC cases were cytologically discriminated accurately, sensitivity, specificity, and accuracy were all 100%. Moreover, the results of leave-one-out cross validation, shown in Figure 7, gave a predicted error rate of (2 + 1)/55 = 0.00545.

DISCUSSION

In this study, the large cell cluster with tight cohesion was confirmed to be a valuable cytologic feature, allowing distinction between LCNECs and SCLCs. Although other reports on cytologic features of LCNECs described that cell cohesion of LCNECs was reduced as in SCLC,[17–22] the difference was highly significant in our series. However, palisade arrangement was described as a one point for cytologic distinction of LCNEC from SCLC,[17–22] and it was considered to be easy to detect tight cell cohesion by light microscope. Therefore, it should be emphasized that focusing on large clusters with tight cohesion is most important for cytologic discrimination between LCNECs and SCLCs.

Several authors showed that tumor cells of LCNECs had similar morphologic features to SCLCs except for cell size, this being significantly larger for LCNECs than SCLCs.[17–22] In these series, a majority of the SCLC cells were less than 120 μm^2 in size, statistically significant as compared with LCNEC cells ($p < 0.0001$). Another characteristic was that most of small cells in SCLC cases had no

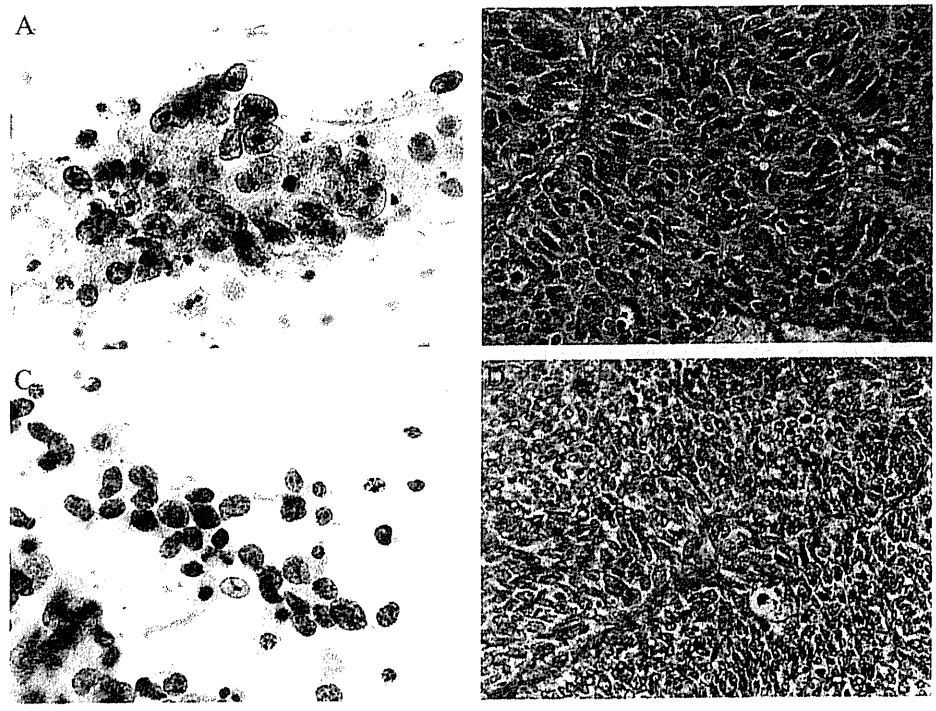

FIGURE 5. Photomicrographs illustrating single cells and tissue architecture in LCNEC and SCLC cases. *A*) Tumor cells ≥120 μm^2 and/or with prominent nucleoli are evident in a cytologic smear of an LCNEC case (Papanicolaou stain, ×100); *B*, nests of LCNEC cells are predominantly composed of large tumor cells with abundant cytoplasm and occasional prominent nucleoli (hematoxylin and eosin stain, ×40); *C*, tumor cells <120 μm^2 without prominent nucleoli are evident in a cytologic smear of an SCLC case (Papanicolaou stain, ×100); *D*, nests of SCLC cells are predominantly composed of small tumor cells with scant cytoplasm without nucleoli (hematoxylin and eosin stain, ×40).

Copyright © 2010 by the International Association for the Study of Lung Cancer

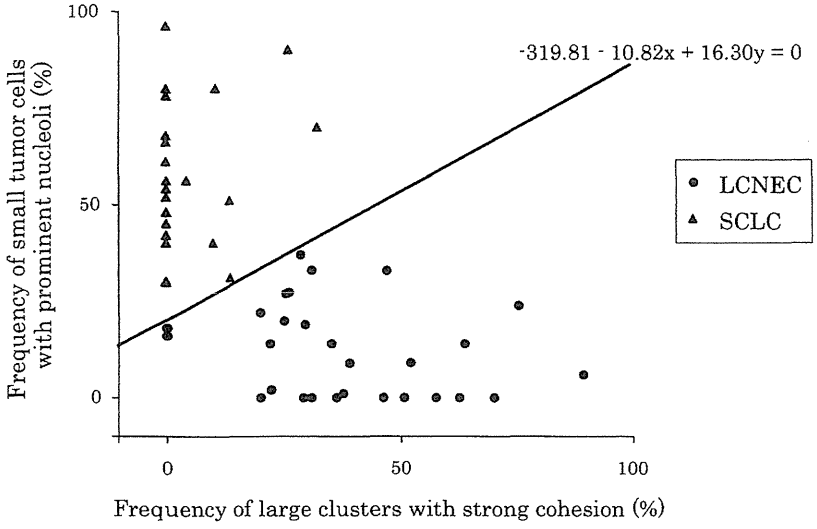

FIGURE 6. Logistic regression for frequencies of small tumor cells without prominent nucleoli and large clusters with tight cohesion. The scatter plot allows clear separation of LCNEC (●) and SCLC cases (▲) by the calculated discriminant line. Therefore, a discriminant model for LCNEC and SCLC, diagnosing as SCLCs if dots exist in the field above the line and as LCNECs if below the line, was made. All SCLC and LCNEC cases were discriminated correctly with the discriminant model based on logistic regression from cytologic frequencies, and sensitivity, specificity, and accuracy were all 100%.

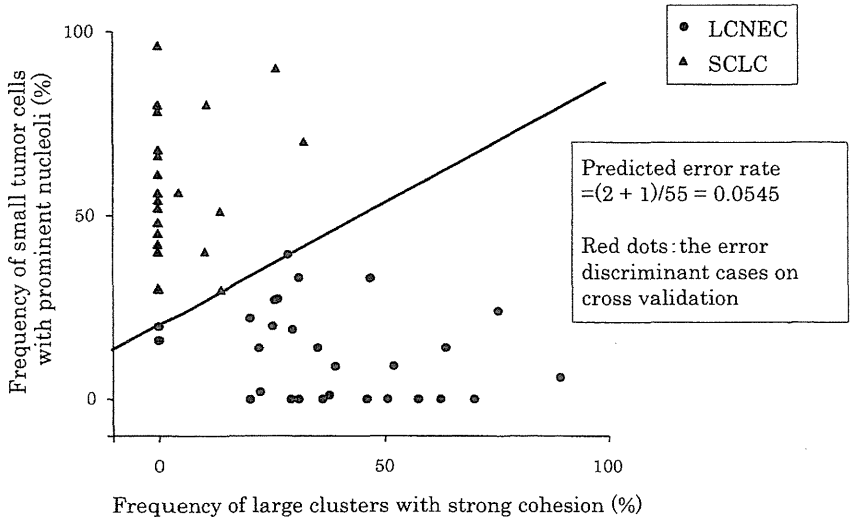

FIGURE 7. Leave-one-out cross validation. Regarding each case as a new case, prediction of the error rate of the discriminant model was analyzed. Red dots show error discriminant cases on cross validation. Two of the LCNEC cases and one SCLC case were discriminated in error with the discriminant model, so that the prediction of error rate of the model was 0.00545.

prominent nucleoli, again being significantly different from LCNECs ($p < 0.0001$). Moreover, although naked nuclei appear to be a significant distinguishing attribute between the two tumor types, it was considered to be inadequate for inclusion in the discriminant model for the following reasons: it is rather difficult to perceive cytoplasm in intact large cells compared with small cells, and naked nuclei was not found in more than 60% of SCLC cases. Therefore, only the frequency of the small cells without prominent nucleoli contributed to cytologic discrimination between LCNEC and SCLC.

To establish accurate cytologic diagnosis of LCNEC using the two cytologic parameters, we established a discriminant model that gave exceedingly good sensitivity, specificity, and accuracy. The current discriminant model, however, does have some problems with routine cytology as follows: complicated procedures for obtaining the two cytologic parameters and necessity of uniform diagnostic criteria among cytopathologists. However, with greater experience of LCNEC cases and grasp of detailed cytologic features, it should be possible to overcome these problems.

In conclusion, our discriminant model based on the cytologic features of large cell clusters with tight cohesion and of small tumor cells without prominent nucleoli should prove a useful aid for distinction between LCNECs and SCLCs particularly. Prospective large-sized studies including other nonsmall cell lung cancers are now required to assess the diagnostic impact of this model with routine cytology.

ACKNOWLEDGMENTS

Supported by a Grant-in-aid from the Ministry of Education, Sports, Culture, Science and Technology grant 20591676, Ministry of Health, Labor and Welfare grant 19-12, and the Vehicle Racing Commemorative Foundation grant.

The authors thank Drs. Masaru Ushijima and Masaaki Matsuura, Bioinformatics Group, Genome Center, Japanese

Copyright © 2010 by the International Association for the Study of Lung Cancer

Foundation for Cancer Research, for helpful advice with the statistical analyses.

REFERENCES

1. Cooper WA, Thourani VH, Gal AA, et al. The surgical spectrum of pulmonary neurocrine neoplasms. *Chest* 2001;119:14–18.
2. Garcia-Yuste M, Matilla JM, Alvarez-Gago T, et al. Prognostic factors in neuroendocrine lung tumors: a Spanish multicenter study. *Ann Thorac Surg* 2000;70:258–263.
3. Jones MH, Virtanen C, Honjoh D, et al. Two prognostically significant subtypes of high-grade lung neuroendocrine tumors independent of small-cell and large-cell neuroendocrine carcinomas identified by gene expression profiles. *Lancet* 2004;363:775–781.
4. Travis WD, Linnoila RI, Tsokos MG, et al. Neuroendocrine tumors of the lung with proposed criteria for large cell neuroendocrine carcinoma. An ultrastructural, immunohistochemical, and flow cytometric study of 35 cases. *Am J Surg Pathol* 1991;15:529–533.
5. Asamura H, Kameya T, Matsuno Y, et al. Neuroendocrine neoplasms of the lung: a prognostic spectrum. *J Clin Oncol* 2006;24:70–76.
6. Dresler CM, Ritter JH, Patterson GA, et al. Clinical-pathologic analysis of 40 patients with large cell neuroendocrine carcinoma of the lung. *Ann Thorac Surg* 1997;63:180–185.
7. Fernandez FG, Battafarano RJ. Large cell neuroendocrine carcinoma of the lung. *Cancer Control* 2006;13:270–275.
8. Hiroshima K, Iyoda A, Shida T, et al. Distinction of pulmonary large cell neuroendocrine carcinoma from small cell lung carcinoma: a morphological, immunohistochemical, and molecular analysis. *Mod Pathol* 2006;19:1358–1368.
9. Iyoda A, Hiroshima K, Nakatani Y, et al. Pulmonary large cell neuroendocrine carcinoma: its place in the spectrum of pulmonary carcinoma. *Ann Thorac Surg* 2007;84:702–707.
10. Iyoda A, Hiroshima K, Toyozaki T, et al. Adjuvant chemotherapy for large cell carcinoma with neuroendocrine features. *Cancer* 2001;92: 1108–1112.
11. Jiang SX, Kameya T, Shoji M, et al. Large cell neuroendocrine carcinoma of the lung: a histologic and immunohistochemical study of 22 cases. *Am J Surg Pathol* 1998;22:526–537.
12. Travis WD, Gal AA, Colby TV, et al. Reproducibility of neuroendocrine lung tumor classification. *Hum Pathol* 1998;29:272–279.
13. Wick MR, Berg LC, Herts MI. Large cell carcinoma of the lung with neuroendocrine differentiation: a comparison with large cell "undifferentiated" pulmonary tumors. *Am J Surg Pathol* 1992;97:796–805.
14. Veronesi G, Morandi U, Alloisio M, et al. Large cell neuroendocrine carcinoma of the lung: a retrospective analysis of 144 surgical cases. *Lung Cancer* 2006;53:111–115.
15. Travis WD, Colby TV, Corrin B, et al. *Histological Typing of Lung and Pleural Tumors*. 3rd Ed. *World Health Organization International Histological Classification of Tumors*. Berlin: Springer Verlag, 1999.
16. Colby TV, Koss MN, Travis WD. *Tumors of the Lower Respiratory Tract. Atlas of Tumor Pathology*. 3rd series. Washington DC: Armed Forces Institute of Pathology, 1995:248–255.
17. Hiroshima K, Abe S, Ebihara Y, et al. Cytological characteristics of pulmonary large cell neuroendocrine carcinoma. *Lung Cancer* 2005;48: 331–337.
18. Iyoda A, Baba M, Hiroshima K, et al. Imprint cytologic features of pulmonary large cell neuroendocrine carcinoma: comparison with classic large cell carcinoma. *Oncol Rep* 2004;11:285–288.
19. Jimenez-Heffernan JA, Lopez-Ferrer P, Vicandi B, et al. Fine-needle aspiration cytology of large cell neuroendocrine carcinoma of the lung: a cytopathologic correlation study of 11 cases. *Cancer* 2008;114:180–186.
20. Kakinuma H, Mikami T, Iwabuchi K, et al. Diagnostic findings of bronchial brush cytology for pulmonary large cell neuroendocrine carcinomas. *Cancer (Cancer Cytopathol)* 2003;99:247–254.
21. Nicholson SA, Ryan MR. A review of cytologic findings in neuroendocrine carcinomas including carcinoid tumor with histologic correlation. *Cancer (Cancer Cytopathol)* 2000;90:148–161.
22. Wiatrowska BA, Krol J, Zakowski MF. Large cell neuroendocrine carcinoma of the lung: proposed criteria for cytologic diagnosis. *Diagn Cytopathol* 2001;24:58–64.
23. Nicholson SA, Beasley MB, Brambilla E, et al. Small cell lung carcinoma (SCLC): a clinicopathologic study of 100 cases with surgical specimens. *Am J Surg Pathol* 2002;26:1184–1197.

Copyright © 2010 by the International Association for the Study of Lung Cancer

The American Journal of Pathology, Vol. 176, No. 4, April 2010
Copyright © American Society for Investigative Pathology
DOI: 10.2353/ajpath.2010.090486

Tumorigenesis and Neoplastic Progression

Function of *EWS-POU5F1* in Sarcomagenesis and Tumor Cell Maintenance

Takashi Fujino,*† Kimie Nomura,‡ Yuichi Ishikawa,‡ Hatsune Makino,§ Akihiro Umezawa,§ Hiroyuki Aburatani,¶ Koichi Nagasaki,‖ and Takuro Nakamura*

From the Divisions of Carcinogenesis, and Pathology,‡ and the Genome Center,‖ The Cancer Institute, Japanese Foundation for Cancer Research, Tokyo; the Department of Pathology,† Faculty of Medicine, Kyorin University, Tokyo; the Department of Reproductive Biology,§ National Institute for Child and Health Development, Tokyo; and the Genome Research Division,¶ Research Center for Advanced Science and Technology, University of Tokyo, Tokyo, Japan*

POU5F1 is a transcription factor essential for the self-renewal activity and pluripotency of embryonic stem cells and germ cells. We have previously reported that *POU5F1* is fused to *EWSR1* in a case of undifferentiated sarcoma with chromosomal translocation t(6;22)(p21;q12). In addition, the *EWS-POU5F1* chimeras have been recently identified in human neoplasms of the skin and salivary glands. To clarify the roles of the *EWS-POU5F1* chimera in tumorigenesis and tumor cell maintenance, we used small-interfering RNA-mediated gene silencing. Knockdown of *EWS-POU5F1* in the t(6;22) sarcoma-derived GBS6 cell line resulted in a significant decrease of cell proliferation because of G1 cell cycle arrest associated with $p27^{Kip1}$ up-regulation. Moreover, senescence-like morphological changes accompanied by actin polymerization were observed. In contrast, *EWS-POU5F1* down-regulation markedly increased the cell migration and invasion as well as activation of metalloproteinase 2 and metalloproteinase 14. The results indicate that the proliferative activity of cancer cells and cell motility are discrete processes in multistep carcinogenesis. These findings reveal the functional role of the sarcoma-related chimeric protein as well as POU5F1 in the development and progression of human neoplasms. *(Am J Pathol 2010, 176:1973–1982; DOI: 10.2353/ajpath.2010.090486)*

POU5F1/OCT4 is an essential transcription factor for the formation and/or maintenance of the inner cell mass of the mammalian blastocyst, the origin of pluripotent embryonic stem (ES) cells.[1–3] Suppression of *POU5F1* expression converts ES cells to trophoblasts, whereas overexpression of *POU5F1* leads to differentiation toward endoderm and mesoderm.[3,4] The self-renewal activity and pluripotency of ES cells are suppressed by knockdown of *POU5F1*.[5] These data suggest that POU5F1 orchestrates target gene expression in a tightly regulated manner during development and cellular differentiation. Also, POU5F1 induces reprogramming of somatic cells into iPS cells in combination with Sox2, c-Myc, and Klf4.[6] Moreover, two factors, either POU5F1 and Klf4 or POU5F1 and c-Myc, are apparently sufficient to generate iPS cells.[7]

In carcinogenesis, up-regulated expression of *POU5F1* is significantly correlated to certain lineages of human malignancies including germ cell tumors and breast and bladder cancer.[8–11] Reactivation of POU5F1 in somatic cells may induce dedifferentiation and may disrupt homeostasis, resulting in malignant transformation. Direct involvement of POU5F1 has been detected in a case of undifferentiated bone sarcoma with t(6;22)(p21;q12) translocation in which *POU5F1* is fused to *EWSR1*.[12] The chimeric *EWS-POU5F1* protein is composed of a transactivation domain of EWS and the entire DNA-binding domain of POU5F1. Ectopic overexpression of the POU5F1 component is achieved by the strong promoter activity of *EWSR1*.[12] Similar gene fusions between *EWSR1* and *POU5F1* have been identified in hidradenoma of the skin and mucoepidermoid carcinoma of the salivary glands.[13] These results underscore the important role of dysregulated *POU5F1* expression in human cancer and the important contributions of *EWS-POU5F1* to the development and maintenance of cancer cells.

In this study, we knocked down *EWS-POU5F1* by using *POU5F1*-specific small-interfering RNAs (siRNAs) in

Supported in part by Grant-in-Aid for Scientific Research on Priority Areas "Integrative Research Toward the Conquest of Cancer" from the Ministry of Education, Culture, Sports, Science, and Technology of Japan, and supported by Kawano Masanori Memorial Foundation for Promotion of Pediatrics.

Accepted for publication December 15, 2009.

Supplemental material for this article can be found on *http://ajp.amjpathol.org*.

Address reprint requests to Takuro Nakamura, M.D., Ph.D., Division of Carcinogenesis, The Cancer Institute, Japanese Foundation for Cancer Research, 3-8-31 Ariake, Koto-ku, Tokyo 135-8550, Japan. E-mail: takuro-ind@umin.net.

the GBS6 cell line established from the t(6;22) undifferentiated sarcoma.[12] Cellular growth was significantly suppressed by *EWS-POU5F1* depletion and was accompanied by up-regulation of $p27^{Kip1}$ expression, and senescence-like morphological alterations were observed. On the other hand, cell motility and invasive capacity were dramatically increased, and promotion of actin polymerization and activation of metalloproteinase (MMP)14 and MMP2 were observed. These results suggest that EWS-POU5F1 promotes proliferation of cancer cells but is dispensable for or even inhibits cell motility and invasiveness. This study provides important insights into EWS-POU5F1 function in carcinogenesis and tumor cell maintenance.

Materials and Methods

Cell Culture

The GBS6 cell line was established from a pelvic bone undifferentiated sarcoma with t(6;22)(p21;q12).[12] The cells were maintained at 37°C under 5% CO_2 in RPMI 1640 medium supplemented with 10% fetal bovine serum and 10 mmol/L of HEPES buffer, pH7.4. NIH3T3, HeLa, and HCT116 cells were grown at 37°C under 5% CO_2 in Dulbecco's modified Eagle's medium supplemented with 10% fetal bovine serum.

RNA Interference and DNA Transfection

RNA interference and DNA transfection experiments were performed by using Lipofectamine 2000 (Invitrogen, Carlsbad, CA). GBS6 cells were seeded on 12-well plates 24 hours before transfection at a density of 1×10^5 or 2.5×10^5 cells per well for siRNAs or plasmid DNAs, respectively. GBS6 cells were then transfected with 60 pmol or 1.6 μg of siRNAs or plasmids, respectively. The following siRNAs were purchased from Qiagen (Hilden, Germany): siRNA-POU5F1-1 (SI00690389) and siRNA-POU5F1-2 (SI026617) and control (non-sil). A FLAG-tagged p27 expression plasmid was a kind gift from Dr. Kei-ichi Nakayama.

Senescence-Associated β-galactosidase Assay

Senescence-associated β-galactosidase was detected histochemically by using a Senescence Detection Kit (Biovision, Mountain View, CA) 4 days after transfection of siRNAs.

Western Blotting

Whole cell lysates were size-fractionated by SDS-polyacrylamide gel electrophoresis and were transferred onto a nitrocellulose membrane. The membrane was blocked with Tris-buffered saline (pH 7.5) containing 0.2% Tween 20 and 5% nonfat dry milk. Primary antibodies used were as follows: goat anti-Oct3/4 (1:500 dilution; C-20, Santa Cruz Biotechnology, Santa Cruz, CA), mouse anti-lamin A/C (1:500 dilution; Santa Cruz Biotechnology), rabbit anti-p27 (1:200 dilution; Santa Cruz Biotechnology), mouse anti-p53 (1:200 dilution; DO-1, Santa Cruz Biotechnology), mouse anti-p21 (1:100 dilution; BD Biosciences, San Diego, CA), mouse anti-Rb (1:500 dilution; IF8, Santa Cruz Biotechnology), rabbit anti-Phospho-Rb (Ser807/811; 1:500 dilution; Cell Signaling Technology, Beverly, MA), mouse anti-cyclin D1 (1:500 dilution; A-12, Santa Cruz Biotechnology), rabbit anti-CDK2 (1:500 dilution; M2, Santa Cruz Biotechnology), rabbit anti-CDK4 (1:500 dilution; H-22, Santa Cruz Biotechnology), rabbit anti-CDK6 (1:500 dilution; C-21, Santa Cruz Biotechnology), mouse anti-MMP14 (1:200 dilution; Daiichi Fine Chemical, Tokyo, Japan), and mouse anti-RhoA (1:200 dilution; Upstate Biotechnology, Temecula, CA). The signals were detected by using appropriate secondary antibodies and an enhanced chemiluminescence kit (GE Health care, Piscataway, NJ).

Flow Cytometric Analysis

Single cell suspensions were permeabilized with 0.1% triton X-100 in PBS, and 50 mg/ml of propidium iodide and 1 mg/ml of RNase A were added. The cell suspensions were then analyzed by using a FACS-calibur flow cytometer (Beckton Dickinson, Franklin Lakes, NJ) and Modifit software (Beckton Dickinson).

Cell Invasion and Migration Assays

A quantitative invasion assay was performed by using a BD BioCoat Matrigel invasion chamber with 8-μm pore size membranes (BD Biosciences) according to the manufacturer's instruction. Briefly, cells incubated with siRNAs or plasmid DNAs for 24 hours were trypsinized and resuspended at a density of 1×10^5 cells per 1 ml of RPMI without serum. Cells (5×10^5) were then loaded onto inserts of the upper chambers. RPMI with 10% fetal bovine serum was added to the lower chambers. After 24 hours of incubation, cells on the upper surface membranes were removed gently with a cotton swab. Cells on the lower surface were stained with Wright-Giemsa solutions and air-dried. Cell migration was also evaluated by using the same chambers without Matrigel by assessing the cell numbers within the lower chamber. The invading or migrating cells were counted, and images were obtained by using an Olympus BX41 microscope with a 20× objective (Olympus, Tokyo, Japan). For the wound healing assay, GBS6 cells were cultured for 48 hours after transfection of siRNAs to reach 90% confluence in 12-well plates. A linear scratch, 100 μm in width, was produced by using a plastic tip. Cells were incubated in growth medium for the indicated period. Images were photographed by using an Olympus IX70 phase contrast microscope. The distance of cell migration from the scratch line was measured in micrometers on the photographs.

Gelatin Zymography

Conditioned media from GBS6 cell cultures were harvested 48 hours after siRNA transfection, loaded on 10% gelatin gels (Invitrogen), and electrophoresed. The gels were stained with 0.25% Coomassie Blue and were destained in 5% acetic acid/10% methanol to visualize bands corresponding to the gelatinolytic activity.

Total RNA Extraction, Conventional RT-PCR, and Real-Time Quantitative RT-PCR

Total RNA extraction, reverse transcription, and RNA quantification were performed according to methods described previously.[14] Conventional RT-PCR was performed by using a Gene Amp 9700 thermal cycler (Applied Biosystems, Foster City, CA). We conducted 40 cycles of three-step PCR (95°C for 30 seconds, 55°C for 1 minute, and 72°C for 1 minute) for miR032-367 locus and 25 cycles of three-step PCR (95°C for 30 seconds, 60°C for 30 seconds, and 72°C for 30 seconds) for actin. The specific forward and reverse primers for optimal amplification were designed as follows: miR302-367 locus, 5′-GGGCTCCCTTCAACTTTAAC-3′ and 5′-ATTCTGTCATTGGCTTAACAATCCATCACC-3′; β-actin, 5′-AGGCATCCTCACCCTGAAGTACCC-3′ and 5′-GCCAGGTCCAGACGCAGG-3′. Real-time RT-PCR was performed by using a 7500 Fast Real-Time PCR System (Applied Biosystems) using the following parameters: 40 cycles of three-step PCR (95°C for 15 seconds, 60°C for 30 seconds, and 72°C for 30 seconds). The specific forward and reverse primers to produce approximately 60-bp amplicons for optimal amplification in real-time PCR were designed as follows: MMP2, 5′-CCGCAGTGACGGAAAGATGT-3′ and 5′-GCCCCACTTGCGGTCAT-3′; MMP14, 5′-CGAGAGGAAGGATGGCAAATT-3′ and 5′-AGGGACGCCTCATCAAACAC-3′; β-actin, 5′-TGGATCAGCAAGCAGGAGTATG-3′ and 5′-GCATTTGCGGTGGACGAT-3′; and miR302-367 locus, 5′-TTTGAGTGTGGTGGTTCCTACCT-3′ and 5′- AGCCAAGAACTGCACACAGTGT-3′.

Actin Staining

GBS6 cells were seeded onto four-chamber culture slides (BD Biosciences) at a density of 3000 cells per well 24 hours after transfection and were incubated for an additional 24 hours in growth medium. Cells were then fixed and stained with phalloidin-rhodamine (Invitrogen). Images were photographed by using a Leica DM6000B laser scanning microscope with a 40× objective (Leica Microsystems, Cambridge, UK).

RhoA Activity Assay

To confirm RhoA activation, the amount of RhoA-GTP bound to the Rhotekin Rho-binding domain (RBD) was determined by using the Rho Activation Assay Kit (Upstate Biotechnology). Forty-eight hours after transfection of siRNAs, whole cell lysates were incubated with Rhotekin RBD-agarose for 45 minutes at 4°C. After washing, agarose beads were resuspended in Laemmli sample buffer, boiled for 5 minutes, and subjected to immunoblotting with an anti-RhoA antibody.

Microarray

The oligonucleotide array Human Genome U133 Plus 2.0 (Affymetrix, Santa Clara, CA), composed of 38,500 human genes and expressed sequence tags, was hybridized with cRNA probes generated from GBS6 cells 4 days after siRNA transfection and was scanned according to the method previously described.[14] The data were deposited in a public database (*http://www.ncbi.nlm.nih.gov/geo*, accession number: GSE12320, last accessed November 5, 2009). Clustering analysis was performed by using dChip software (*http://biosun1.harvard.edu/complab/dchip/* last accessed October 14, 2009). The gene network was analyzed by Webgestalat (*http://bioinfo.vanderbilt.edu/webgestalt/* last accessed October 31, 2009).

Statistical Analysis

Results were evaluated statistically by using Student's *t*-test. A value of $P < 0.05$ was considered significant.

Results

EWS-POU5F1 *Knockdown Induces p27^{Kip1} Up-Regulation and G1 Arrest*

The GBS6 cell line was established from a t(6;22) undifferentiated sarcoma that expressed the chimeric *EWS-POU5F1* but not wild-type *POU5F1*.[12] To investigate the biological role of *EWS-POU5F1*, we knocked down *EWS-POU5F1* in GBS6 cells by RNA interference. Effective knockdown of *EWS-POU5F1* on 2 days after transfection was confirmed for two independent *POU5F1*-specific siRNAs (Figure 1A, 88.3% of reduction by siRNA-1 and 85.9% by siRNA-2). The effects of the two siRNAs were similar to each other in every experiment, and the results using siRNA-POU5F1-1 are exhibited subsequently as a representative.

Suppression of *EWS-POU5F1* in GBS6 cells was significantly inhibited proliferation, the cell numbers being 58% or 54% of those treated with a control siRNA on day 2 or day 4, respectively (Figure 1B). A terminal deoxynucleotidyl transferase-mediated dUTP nick-end labeling assay did not show an apparent increase of apoptotic cells during treatment with RNA interference (data not shown). This result suggests that the suppression of cell growth might be because of inhibition of the cell cycle. Flow cytometric analysis demonstrated that knockdown of *EWS-POU5F1* significantly decreased the S-phase population and increased the G1 fraction compared with the control (Figure 1C), indicating that cell growth of GBS6 was suppressed because of G1 arrest.

We next examined the expression of a series of cell cycle regulators. Increased expression of p27 was observed in GBS6 cells during *EWS-POU5F1* knockdown (Figure 1D, left). An RT-PCR experiment showed no significant decrease of *p27* mRNA during *EWS-POU5F1*

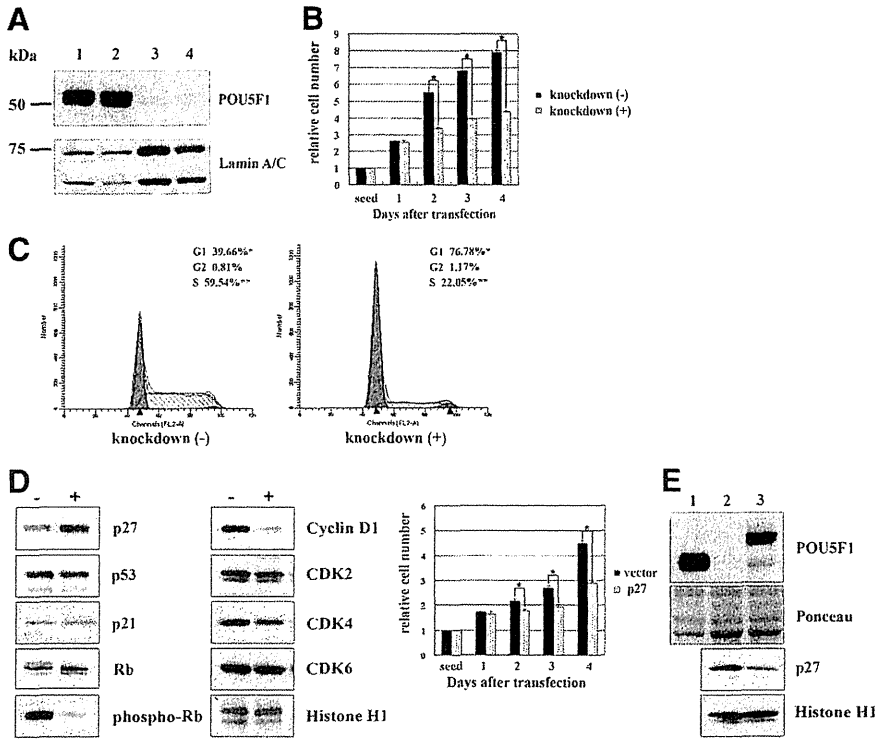

Figure 1. Knockdown of *EWS-POU5F1* inhibits proliferation of GBS6 cells accompanied by G1 cell cycle arrest and up-regulation of p27. **A:** RNA interference. GBS6 cells were transfected with control or *POU5F1* siRNAs and harvested 2 days after transfection; lysates were subjected to Western blotting by using anti-POU5F1 antibody. Lamin A/C was used as a control. **lane 1**, wild-type; **lane 2**, negative control siRNA (non-sil); **lane 3**, POU5F1 siRNA-1; **lane 4**, POU5F1 siRNA-2. **B:** Proliferation assay of GBS6 cells treated with non-sil or POU5F1 siRNA. Mean of relative cell numbers ± SE of three independent experiments are presented (*$P < 0.005$). **C:** Flow cytometric analysis of GBS6 cells treated with siRNAs. Average percentages of G1, G2, and S phases in three experiments are indicated. *$P < 0.005$. **D:** Western blotting of GBS6 cells transfected with control (−) or POU5F1 (+) siRNAs by using antibodies specific for the indicated protein. Histone H1 was used as a loading control (**left**); proliferation assay (**right**) of GBS6 cells in which p27 was introduced. Mean of relative cell numbers ± SE of three independent experiments are presented (*, **$P < 0.005$). **E:** Western blotting of GBS6 cells and NIH3T3 cells transfected with an empty or *EWS-POU5F1* vectors by using anti-POU5F1 or anti-p27. **Lane 1**, GBS6 cells; **lane 2**, NIH3T3 treated with an empty vector; and **lane 3**, NIH3T3 treated with an *EWS-POU5F1* expression vector. Ponceau staining and Histone H1 were used as a loading control.

suppression (data not shown), suggesting that the change might be indirect and *p27* was not transcriptionally regulated by EWS-POU5F1. During knockdown, phosphorylation of Rb protein on Ser807/811 was significantly decreased, whereas expression of total Rb protein remained unchanged (Figure 1D, left). Expression of p21 and p53 was not affected (Figure 1D, left). In addition, a comparative genomic hybridization analysis revealed a homozygous loss of $p16^{INK4A}/p14^{ARF}$ (Supplemental Figure S1, see *http://ajp.amjpathol.org*). A significant decrease of cyclin D1 expression was also noted (Figure 1D, left). On the other hand, expression of CDK2, CDK4, and CDK6 was unchanged (Figure 1D, left).

Exogenous introduction of *p27* into GBS6 cells resulted in 82% and 61% decreased proliferation compared with the transfected controls on days 2 and 4, respectively (Figure 1D, right). Conversely, exogenous expression of *EWS-POU5F1* in NIH3T3 cells markedly depleted p27 (Figure 1E). However, expression of *EWS-POU5F1* did not affect proliferation of NIH3T3 cells, suggesting that the effect might be cell context-dependent. Taken together, these results indicate that EWS-POU5F1 supports tumor cell growth, at least in part, through down-regulating the $p27^{Kip1}$ activity.

Induction of the Senescence-Like Morphology by EWS-POU5F1 *Knockdown*

GBS6 cells possess a short spindle-shaped morphology with a narrow cytoplasm and a small nucleus with rough heterochromatin (Figure 2A, left), reflecting the original phenotype *in vivo*.[12] After introduction of *POU5F1*-specific siRNAs, we observed prompt enlargement of GBS6 cell bodies. Most GBS6 cells demonstrated large and flat cytoplasms as well as enlarged nuclei with fine chromatins 4 days after siRNA transfection. This morphology mimicked that observed in cellular senescence (Figure 2A, right). Most of the GBS6 cells enlarged by *EWS-POU5F1* knockdown expressed senescence-associated β-galactosidase (Figure 2B), a well-established biomarker of senescence.[15] However, senescence-associated heterochromatin foci, another biomarker of senescence,[16] were not observed (data not shown). Importantly, the enlarged GBS6 phenotype (and growth arrest) mediated by *POU5F1*-specific siRNAs disappeared 10 days after transfection when *EWS-POU5F1* expression returned (data not shown). Thus, the change was transient and reversible. These data suggest that the phenotypic changes were not because of senescence but rather indicated G1 arrest. Interestingly, overexpression of $p27^{Kip1}$ did not induce morphological changes in GBS6 cells (data not shown), indicating that different molecular pathways downstream of EWS-POU5F1 are responsible for the senescence-like morphologies.

Drastic modification of the cytoskeleton was also observed in siRNA-treated enlarged GBS6 cells. Phalloidin staining revealed prominent networks of F-actin throughout the cytoplasm of siRNA-treated cells (Figure 2C, right). Control GBS6 cells showed only a small amount of actin fibers in the cytoplasmic rim (Figure 2C, left). A close link between actin polymerization and a small G protein Rho has been reported.[17] Indeed, a GTP-bound activated form of RhoA protein was apparently increased on *EWS-POU5F1* knockdown (Figure 2D). These data indicate that EWS-POU5F1 affected the RhoA signaling pathway and morphology of tumor cells by modulating the actin fiber network. Finally, transfection of *POU5F1*-specific siRNA into HeLa cells that do not express *POU5F1* did not affect cell morphology (Figure 2E), indi-

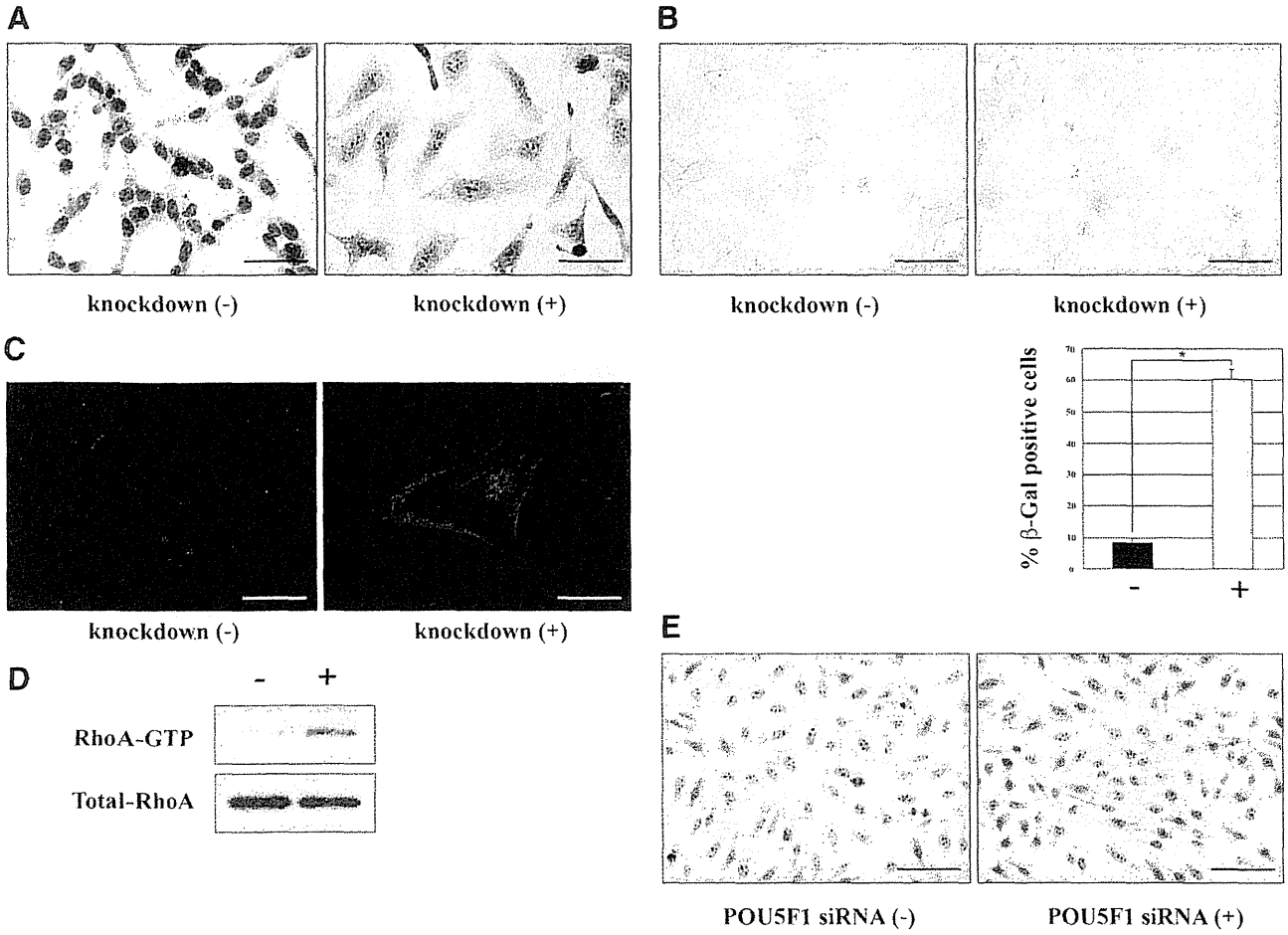

Figure 2. Morphological changes and actin polymerization in siRNA-treated GBS6 cells. **A:** Photomicrographs of GBS6 cells transfected with control siRNA or *POU5F1*-specific siRNA. Papanicolau staining, ×400 original magnification. Scale bars = 100 μm. **B:** Senescence-associated β-galactosidase (SA-β-Gal) assay 4 days after transfection of siRNAs. Original magnification, ×400. Scale bars = 100 μm. The columns indicate mean % SA-β-Gal-positive cells in three independent experiments (*$P < 0.005$). **C:** Enhanced actin polymerization in *EWS-POU5F1* silent GBS6 cells. F-actin was visualized by phalloidin-rhodamine staining. Original magnification, ×400. Scale bars = 100 μm. **D:** Increased RhoA-GTP in *EWS-POU5F1* silenced GBS6 cells (+) compared with control (−). **E:** *POU5F1* knockdown does not affect morphology of HeLa cells. Papanicolau staining, ×200 original magnification. Scale bars = 100 μm.

cating that the above findings are not because of non-specific effects of *POU5F1* siRNAs.

Knockdown of EWS-POU5F1 *Promotes Cell Migration and Invasion*

Uncontrolled proliferation and metastatic activities are important biological characteristics of cancer.[18] Indeed, in the t(6;22) sarcoma case, the patient died of multiple pulmonary metastases.[12] Therefore, it is intriguing to clarify whether EWS-POU5F1 promotes cell migration and invasiveness. Migration and invasion of GBS6 cells treated with siRNA for *EWS-POU5F1*were assessed in a Matrigel invasion assay. *EWS-POU5F1* knockdown resulted in marked increases in migration and invasion activities compared with the control GBS6 cells (Figure 3A and Table 1). The original GBS6 cells rarely migrated *in vitro*; however, the number of cells migrating in the absence of EWS-POU5F1 increased more than 50-fold. The increase in cell motility after *EWS-POU5F1* knockdown was also confirmed by a wound healing assay, showing that GBS6 cells with *EWS-POU5F1* knockdown migrated 2.5-fold faster than the control cells (Figure 3B).

We next asked whether the enhanced invasiveness of GBS6 cells in Matrigel was solely because of increased cell motility or whether invasiveness itself was also accelerated. Because cell invasion activity is closely associated with increased metalloproteinase activity,[19,20] MMP2 and MMP9 activities were assessed by gelatin zymography. The zymogram exhibited a significant increase of the gelatinolytic activity of MMP2, whereas the MMP9 activity was not altered (Figure 3C, top). MMP14/MT1-MMP, a membrane-type MMP, activates pro-MMP2 in collaboration with a tissue inhibitor of metalloproteinase 2.[19,21] An immunoblot analysis demonstrated increased expression of the MMP14 protein (Figure 3C, bottom), consistent with promotion of MMP2 activity. Thus, *EWS-POU5F1* knockdown increased cell motility and also enhanced invasiveness through accelerated degradation of matrix by MMPs.

Real-time quantitative RT-PCR showed that expression of MMP2 and MMP14 was also increased at the RNA level (Figure 3D), suggesting that *EWS-POU5F1* may also

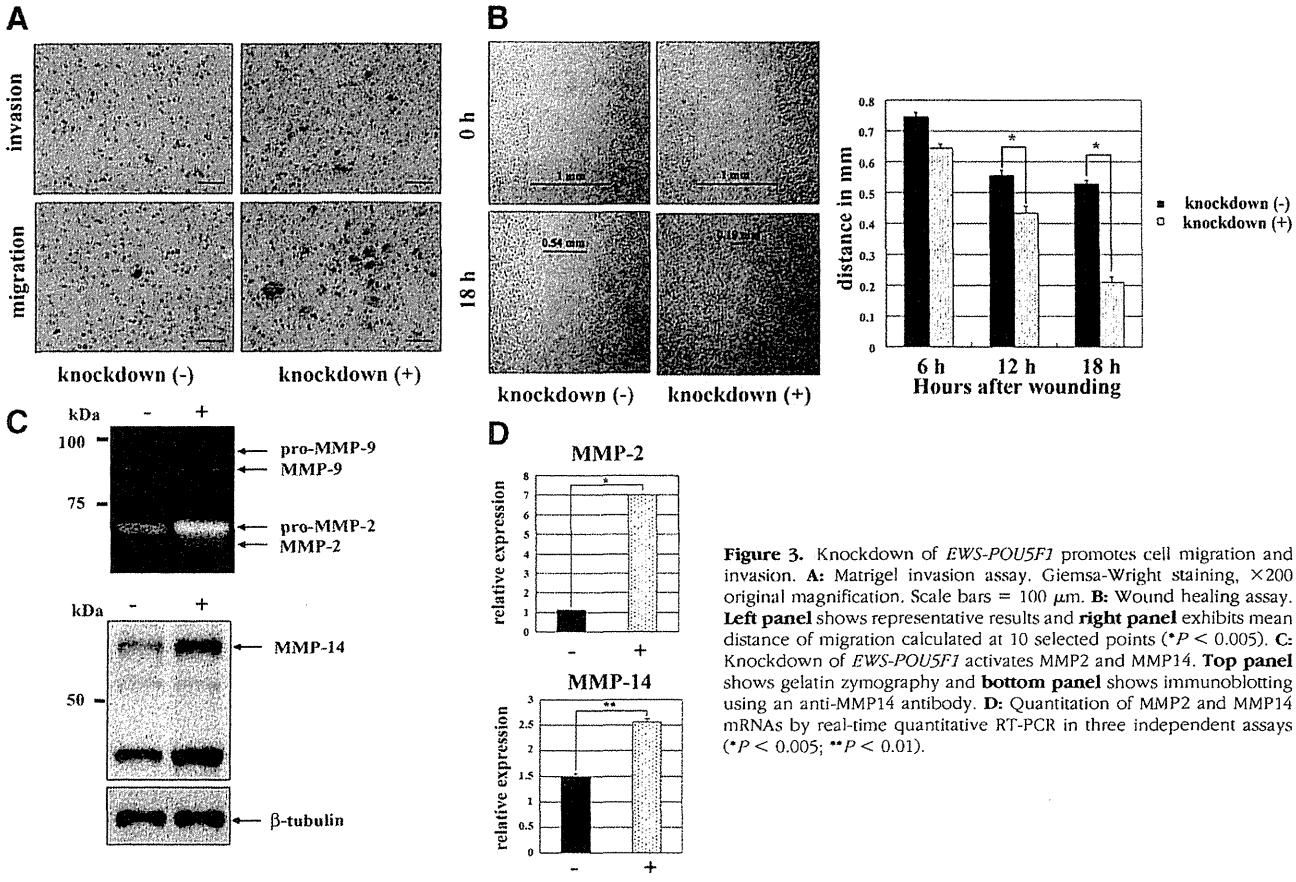

Figure 3. Knockdown of *EWS-POU5F1* promotes cell migration and invasion. **A:** Matrigel invasion assay. Giemsa-Wright staining, ×200 original magnification. Scale bars = 100 μm. **B:** Wound healing assay. **Left panel** shows representative results and **right panel** exhibits mean distance of migration calculated at 10 selected points (*$P < 0.005$). **C:** Knockdown of *EWS-POU5F1* activates MMP2 and MMP14. **Top panel** shows gelatin zymography and **bottom panel** shows immunoblotting using an anti-MMP14 antibody. **D:** Quantitation of MMP2 and MMP14 mRNAs by real-time quantitative RT-PCR in three independent assays (*$P < 0.005$; **$P < 0.01$).

regulate MMP expression directly or indirectly. The Matrigel invasion assay was also performed by using HeLa cells after introduction of the *EWS-POU5F1* expression vector. Cellular invasiveness was again suppressed (Figure 4A and Table 1; $P < 0.01$), though cell migration was decreased only moderately. In addition, depletion of MMP14 protein was demonstrated by introduction of *EWS-POU5F1* into both HeLa and HCT116 colon carcinoma cells (Figure 4B). Overexpression of *EWS-POU5F1* did not affect the expression level of p27, MMP2, or MMP9 in HeLa or HCT116 cells (data not shown). These results suggest that EWS-POU5F1 suppresses cellular motility and invasion in the broad cellular context. In contrast, overexpression of $p27^{Kip1}$ did not affect either cell migration or invasion (Table 1), clearly indicating that cell motility/invasiveness is modulated in a p27-independent manner in GBS6 cells and that simple growth suppression is not sufficient to enhance the invasive activity of tumor cells.

Modulation of the Gene Expression Profile by EWS-POU5F1 *Suppression*

To investigate important downstream molecules regulated by EWS-POU5F1, alteration of global gene expression profiles by *EWS-POU5F1* knockdown was examined. We compared RNAs derived from *POU5F1*-specific siRNA-treated and control GBS6 cells (4 days after siRNA treatment) by using 54,676 probe sets of Affymetrix GeneChip Human Genome U133 Plus 2.0. We identified 98 probe sets (80 genes), the expression of which was increased more than 1.5-fold, and 55 probe sets (45 genes), the expression of which was decreased more than 1.5-fold (Figure 5A and Supplemental Table S1 at *http://ajp.amjpathol.org*). The genes whose expression was modified significantly were then classified according to gene ontology categories (Figure 5B). Interestingly,

Table 1. Invasiveness and Migration of GBS6 and HeLa Cells

	EWS-POU5F1 knockdown in GBS6		*p27* expression in GBS6		*EWS-POU5F1* expression in HeLa	
Cells and treatment	−	+	−	+	−	+
No. invasion	0.3 ± 0.4	101 ± 19*	0	0	1108 ± 85	357 ± 64*
No. migration	9.3 ± 3.2	>500*	11.1 ± 1.1	3.0 ± 0.7	3628 ± 401	1725 ± 229

Mean values ± SE of cell numbers of invasion and migration per 5 × 10^5 cells are exhibited.
*$P < 0.01$ versus control (−).

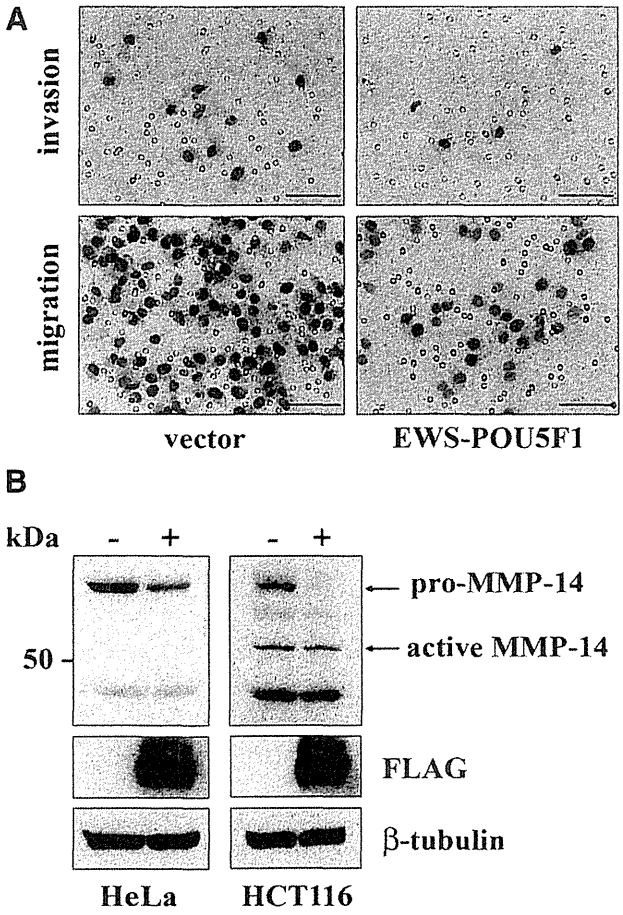

Figure 4. Inhibition of cell migration and invasion by EWS-POU5F1 in HeLa cells. **A:** Matrigel invasion assay. Giemsa-Wright staining, ×200 original magnification. Scale bars = 100 μm. **B:** Immunoblotting of HeLa cells transfected with control (−) or *EWS-POU5F1* (+) expression vectors using anti-MMP14 (**top**), anti-FLAG (**middle**), and anti-β-tubulin (**bottom**).

23.8% of up-regulated genes were involved in cell motility, invasion, or cytoskeleton, consistent with the remarkable alteration of the phenotypes in GBS6 cells. In addition, 13.3% of down-regulated and 13.8% of up-regulated genes belong to differentiation and development categories, indicating importance of the POU5F1 function in pluripotency. However, *EWS-POU5F1* knockdown did not induce GBS6 cells to differentiate toward any specific lineage.

Representative differentially expressed genes of interest belonging to motility, adhesion/invasiveness, morphology/cytoskeleton, mesodermal differentiation, and growth suppression categories are shown in Figure 5C. In motility and adhesion/invasiveness categories, up-regulation of *MMP2* was again observed, though *MT1-MMP* was up-regulated only marginally. We also noted up-regulation of *CAV1*, the mutation of which is associated with mammary carcinoma invasiveness.[22] In addition, another up-regulated gene, *F2R*, has been reported as overexpressed in human cancers with high metastatic potency.[23] Down-regulation of *ELMO1* is intriguing because it is required for promoting phagocytosis and cell shape changes.[24]

A number of genes involved in the differentiation process were up-regulated by *EWS-POU5F1* knockdown. *MGP*, *LBH*, *JUN*, *MYOF*, *CTGF*, and *MESDC2* are involved in mesodermal differentiation (Figure 5C and Supplemental Table S1 at *http://ajp.amjpathol.org*). The mesodermal origin of t(6;22) sarcoma was also supported by the fact that a number of genes encoding extracellular matrix proteins were also up-regulated. However, any specific differentiation toward muscle, bone, cartilage, or adipocytes was not supported by gene expression profiling.

Four putative tumor suppressors, *IGFBP7*, *HTRA1*, *TGFBR2*, and *SOCS3*, were up-regulated by *EWS-POU5F1* knockdown.[25–28] Although it remains unclear whether these genes are the direct targets of EWS-POU5F1, modified expression of these genes should be noted in addition to the altered state of p27, cyclin D1, and Rb. In summary, expression profiling provided important information on the molecular networks affected by the oncogenic function of EWS-POU5F1.

EWS-POU5F1 Up-Regulates the ES Cell-Specific miR302-367 Cluster

MicroRNAs (miRNAs) are noncoding RNAs consisting of approximately 22 nucleotides, which posttranscriptionally regulate mRNAs. They are important in development and differentiation, and abnormal expression of miRNAs has been reported in various neoplasms.[29,30] The miR302-367 cluster has been identified recently as ES cell-specific, and the cluster is transcriptionally regulated by Nanog, POU5F1, Sox2, and Rex1.[31,32] RT-PCR analysis revealed remarkable down-regulation of the miR302-367 cluster during knockdown of *EWS-POU5F1* (Figures 6A and 6B), suggesting that chimeric EWS-POU5F1, like wild-type POU5F1, may regulate miR302-367. The result strongly suggests that EWS-POU5F1 regulates downstream genes not only by its direct DNA binding but also through modulating the expression of miRNA.

Discussion

In the present study we show that EWS-POU5F1 enhances cellular proliferation of GBS6 sarcoma cells. Knockdown of *EWS-POU5F1* caused GBS6 cells to arrest in the G1 phase of the cell cycle. We also noted up-regulation of $p27^{Kip1}$, down-regulation of cyclin D1, and diminished phosphorylation of Rb protein. The tumor suppressor $p27^{Kip1}$ is a CDK2 inhibitor, and it inhibits the cell cycle at the G1/S transition.[33] It is likely that $p27^{Kip1}$ functions downstream from EWS-POU5F1 in oncogenic transformation. In support of this idea, exogenous introduction of $p27^{Kip1}$ blocked proliferation of GBS6 cells.

During suppression of *EWS-POU5F1*, GBS6 cells showed morphological changes similar to those seen in cellular senescence (eg, spreading of the cytoplasm, marked enlargement of cell size, and expression of senescence-associated β-galactosidase, a hallmark of senescence).[15] However, the lack of senescence-associated heterochromatin foci[16] and the reversible nature of the G1 arrest suggest that the change induced by *EWS-POU5F1* knockdown differs from senescence. Loss of $p16^{INK4A}$ might protect GBS6 cells from senescence,

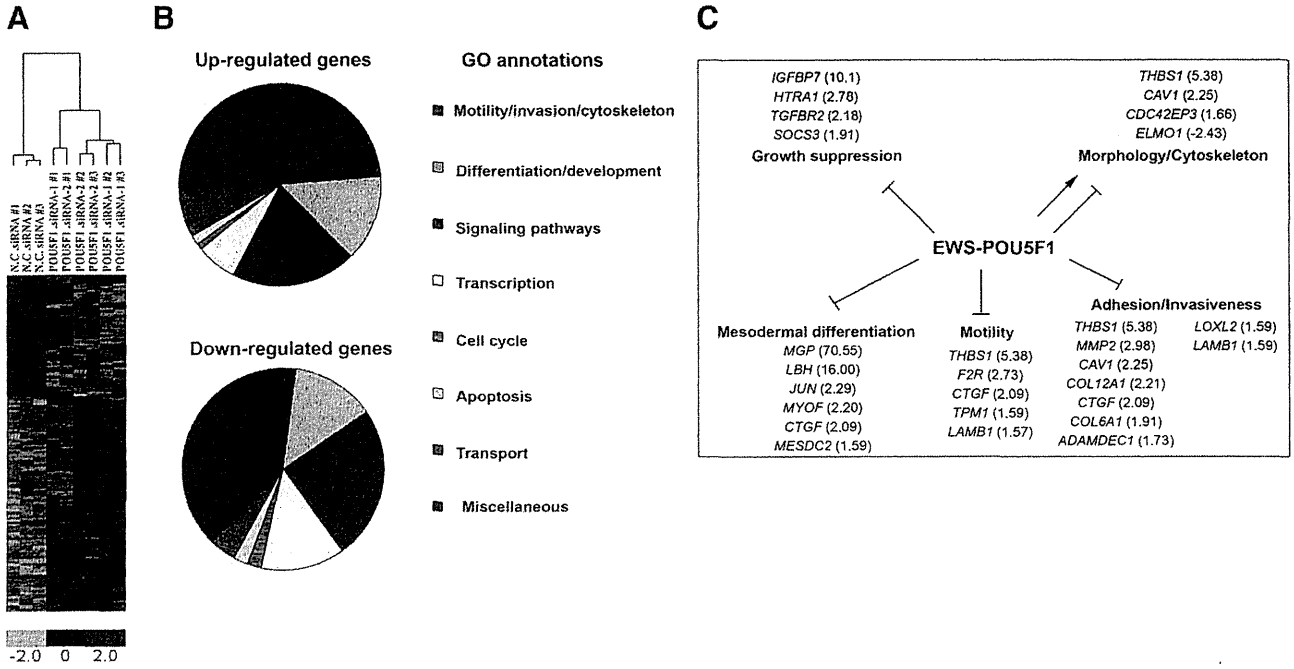

Figure 5. Gene clustering analysis across the compared populations. **A:** Heat map shows the expression of EWS-POU5F1 regulated genes in GBS6 cells treated with negative control siRNA or *POU5F1*-specific siRNAs. Up-regulated and down-regulated genes are presented in red and green, respectively. **B:** Pie charts show the distribution of the 80 up-regulated and 45 down-regulated genes in GBS6 cells transfected with *POU5F1* siRNAs according to gene ontology (GO) annotations. **C:** Prediction of the major signaling pathways affected by EWS-POU5F1. Lower bound of fold changes in each gene are indicated in parentheses.

and senescence-like morphological changes might be achieved by alteration of the actin fiber network.

The inhibitory role of EWS-POU5F1 in cell migration and invasion was unexpected. It is very likely that multiple molecular processes were responsible for increased motility and invasiveness of GBS6 cells treated with *POU5F1* siRNAs. It has been reported that RhoA activation induces actin polymerization[17] that is causatively related to cancer cell invasion and migration.[34] Paradoxical promotion of tumor invasiveness related to $p27^{Kip1}$-dependent G1 arrest has been reported in malignant melanoma with Mitf activation in which Mitf promotes melanoma proliferation by down-regulating $p27^{Kip1}$ but suppresses tumor cell invasion by the Dia1-dependent pathway.[35] Furthermore, $p27^{Kip1}$ supports cell motility through modulation of the RhoA pathway.[36] In GBS6 cells, however, introduction of $p27^{Kip1}$ affected neither cell mobility/invasiveness nor morphological changes. Those results suggest that there might be a $p27^{Kip1}$-independent pathway in RhoA activation and actin polymerization. MMP2 and MT1-MMP, which were up-regulated by knockdown of *EWS-POU5F1*, are candidate upstream regulators of RhoA because recent studies indicate these MMPs induce RhoA activation in osteosarcoma and vascular endothelial cells.[37,38] Moreover, our study indicates that increased cell motility was not a simple consequence of growth suppression. Furthermore, the present results raise an important concern for the treatment of cancer in general. That is, when treatment suppresses the expression of oncogenic transcription factors, inhibition of tumor growth might be accompanied by enhanced tumor cell invasion and metastasis.

Carcinogenesis is a multistep process that requires multiple genetic and epigenetic alterations.[39] Therefore, the fusion of *EWSR1* and *POU5F1* is not sufficient for complete carcinogenesis, and t(6;22) tumors possess additional mutations such as *p16/p14* loss. Our prelimi-

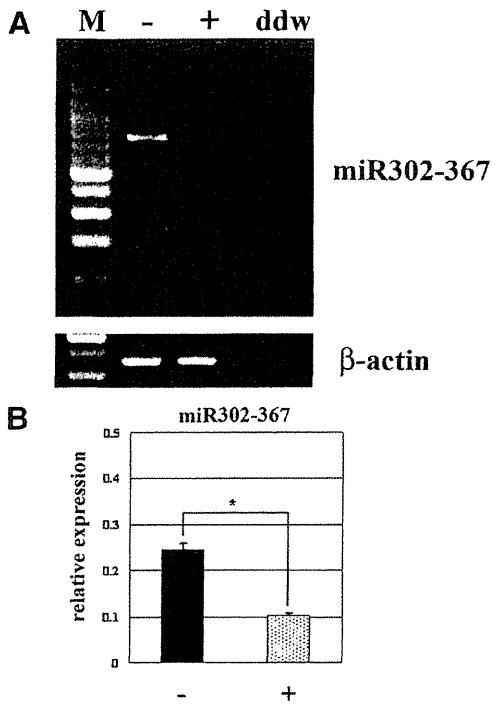

Figure 6. **A:** RT-PCR analysis of miR302-367 in GBS6 cells transfected with control (−) or POU5F1 (+). β-actin was amplified to confirm qualities and quantities of RNA. **B:** Real time quantitative RT-PCR analysis of miR302-367. Average expression was calculated in three independent experiments (*$P < 0.005$).

nary study demonstrated that retrovirus-mediated gene transfer of *EWS-POU5F1* could immortalize but not induce full transformation of murine mesenchymal stem cells (M. Tanaka and T. Nakamura, unpublished observation). Identification of genes cooperative with *EWS-POU5F1* for carcinogenesis is important, and genetic analysis including mutagenesis experiments will provide useful information for understanding the mechanism of *POU5F1*-induced carcinogenesis. In addition, our study suggests that tumor progression toward invasive properties may be caused by genes that do not cooperate with *EWS-POU5F1* but may even counteract *EWS-POU5F1*.

It is intriguing to define important EWS-POU5F1 target genes in carcinogenesis. Because POU5F1/Oct3/4 is a transcriptional regulator, it is likely that the fusion to EWS modulates the nature of its regulatory activities for downstream target genes. Previous studies suggested that POU5F1 acquires the enhanced transcriptional activity by addition of the EWS N-terminal domain.[13,40] The target genes for POU5F1 have been extensively investigated by using ES cells.[4,41,42] In these studies POU5F1 is found associated with SOX2 and/or Nanog, both of which are also expressed in GBS6 cells (data not shown). However, the down-regulated genes in *EWS-POU5F1* knockdown GBS6 cells did not always overlap with POU5F1 target genes in ES cells, probably because of the different cellular context between ES cells and sarcoma cells. Alternatively, the addition of the EWS N-terminal domain may alter the binding specificity of POU5F1 to the target sequences. Nevertheless, it is still possible that there are common target genes for both EWS-POU5F1 and wild-type POU5F1. In a comparison between genes showing altered expression on *EWS-POU5F1* knockdown in the present study and the genes detected in chromatin immunoprecipitation (ChIP)-on-chip or chromatin immunoprecipitation-paired-end ditag (ChIP-PET) studies,[41,42] *INSIG1*, *EPHA4*, *DHCR7*, *ANKS1B*, *ANO4*, *RDH10*, *PHF19*, *BNIP3*, and *TRIB1* are good candidates for common target genes of POU5F1 or EWS-POU5F1 in organogenesis or sarcomagenesis. In addition, the miR302-367 cluster has been identified as a target of ES cell-associated transcription factors, including POU5F1.[32] Down-regulation of miR302-367 on *EWS-POU5F1* knockdown strongly suggests that EWS-POU5F1 regulates gene expression by recognition of a target sequence as well as miRNA-mediated mRNA inhibition. In fact, overexpression of miR302 induces cell cycle progression of ES cells.[43] Interestingly, miR302 represses protein expression of cyclin D1 in ES cells, the opposite effect for EWS-POU5F1 in GBS6 cells, suggesting cell context-dependent function of the miR302-467 cluster. Further studies are needed to identify key downstream molecules controlling cell proliferation and/or cell motility and invasiveness.

Acknowledgments

We thank Dr. Kei-ichi Nakayama for providing a human p27 expression vector, Dr. Eiji Hara and Dr. Akiko Takahashi for valuable discussion, and Ms. Sayuri Amino-Shibuya and Ms. Rie Furuya for technical assistance.

References

1. Schöler HR, Dressler GR, Balling R, Rohdewohld H, Gruss P: Oct-4: a germline-specific transcription factor mapping to the mouse t-complex. EMBO J 1990, 9:2185–2195
2. Nichols J, Zevnik B, Anastassiadis K, Niwa H, Klewe-Nebenius D, Chambers I, Schöler H, Smith A: Formation of pluripotent stem cells in the mammalian embryo depends on the POU transcription factor Oct4. Cell 1998, 95:379–391
3. Niwa H, Miyazaki J, Smith AG: Quantitative expression of Oct-3/4 defines differentiation, dedifferentiation or self-renewal of ES cells. Nat Genet 2000, 24:372–376
4. Matoba R, Niwa H, Masui S, Ohtsuka S, Carter MG, Sharov AA, Ko MS: Dissecting Oct3/4-regulated gene networks in embryonic stem cells by expression profiling. PLoS ONE 2006, 1:e26
5. Ivanova N, Dobrin R, Lu R, Kotenko I, Levorse J, DeCoste C, Schafer X, Lun Y, Lemischka IR: Dissecting self-renewal in stem cells with RNA interference. Nature 2006, 442:533–538
6. Takahashi K, Yamanaka S: Induction of pluripotent stem cells from mouse embryonic and adult fibroblast cultures by defined factors. Cell 2006, 126:1–14
7. Kim JB, Zaehres H, Wu G, Gentile L, Ko K, Sebastiano V, Araúzo-Bravo MJ, Ruau D, Han DW, Zenke M, Schöler HR: Pluripotent stem cells induced from adult neural stem cells by reprogramming with two factors. Nature 2008, 454:646–650
8. Jin T, Branch DR, Zhang X, Qi S, Youngson B, Goss PE: Examination of POU homeobox genes in breast cancer cells. Int J Cancer 1999, 81:104–112
9. Gidekel S, Pizov G, Bergman Y, Pikarsky E: Oct3/4 is a dose-dependent oncogenic fate determinant. Cancer Cell 2003, 4:361–370
10. Looijenga LH, Stoop H, de Leeuw HP, de Gouveia Brazao CA, Gillis AJ, van Roozendaal KE, van Zoelen EJ, Weber RF, Wolffenbuttel KP, van Dekken H, Honecker F, Bokemeyer C, Perlman EJ, Schneider DT, Kononen J, Sauter G, Oosterhuis JW: POU5F1 (OCT3/4) identifies cells with pluripotent potential in human germ cell tumors. Cancer Res 2003, 63:2244–2250
11. Atlasi Y, Mowla SJ, Ziaee SA, Bahrami AR: OCT-4, an embryonic stem cell marker, is highly expressed in bladder cancer. Int J Cancer 2007, 120:1598–1602
12. Yamaguchi S, Yamazaki Y, Ishikawa Y, Kawaguchi N, Mukai H, Nakamura T: EWSR1 is fused to POU5F1 in a bone tumor with translocation t(6;22)(p21;q12). Genes Chromosomes Cancer 2005, 43:217–222
13. Möller E, Stenman G, Mandahl N, Hamberg H, Mölne L, van den Oord JJ, Brosjö O, Mertens F, Panagopoulos I: POU5F1, encoding a key regulator of stem cell pluripotency, is fused to EWSR1 in hidradenoma of the skin and mucoepidermoid carcinoma of the salivary glands. J Pathol 2008, 215:78–86
14. Kawamura-Saito M, Yamazaki Y, Kaneko K, Kawaguchi N, Kanda H, Mukai H, Gotoh T, Motoi T, Fukayama M, Aburatani H, Takizawa T, Nakamura T: Fusion between CIC and DUX4 up-regulates PEA3 family genes in Ewing-like sarcomas with t(4;19)(q35;q13) translocation. Hum Mol Genet 2006, 15:2125–2137
15. Lundberg AS, Hahn WC, Gupta P, Weinberg RA: Genes involved in senescence and immortalization. Curr Opin Cell Biol 2000, 12:705–709
16. Narita M, Nũnez S, Heard E, Narita M, Lin AW, Hearn SA, Spector DL, Hannon GJ, Lowe SW: Rb-mediated heterochromatin formation and silencing of E2F target genes during cellular senescence. Cell 2003, 113:703–716
17. Ridley AJ, Hall A: The small GTP-binding protein rho regulates the assembly of Focal adhesions and actin stress fibers in response to growth factors. Cell 1992, 70:401–410
18. Hanahan D, Weinberg RA: The hallmarks of cancer. Cell 2000, 100:57–70
19. Seiki M: The cell surface: the stage for matrix metalloproteinase regulation of migration. Curr Opin Cell Biol 2002, 14:624–635
20. Seiki M, Mori H, Kajita M, Uekita T, Itoh Y: Membrane-type 1 matrix metalloproteinase and cell migration. Biochem Soc Symp 2003, 70:253–262
21. Seiki M, Koshikawa N, Yana I: Role of pericellular proteolysis by membrane-type 1 matrix metalloproteinase in cancer invasion and angiogenesis. Cancer Metastasis Rev 2003, 22:129–143
22. Bonuccelli G, Casimiro MC, Sotgia F, Wang C, Liu M, Katiyar S, Zhou J, Dew E, Capozza F, Daumer KM, Minetti C, Milliman JN, Alpy F, Rio MC,

Tomasetto C, Mercier I, Flomenberg N, Frank PG, Pestell RG, Lisanti MP: Caveolin-1 (P132L), a common breast cancer mutation, confers mammary cell invasiveness and defines a novel stem cell/metastasis-associated gene signature. Am J Pathol 2009, 174:1650–1662
23. Boire A, Covic L, Agarwal A, Jacques S, Sherifi S, Kuliopulos A: PAR1 is a matrix metalloprotease-1 receptor that promotes invasion and tumorigenesis of breast cancer cells. Cell 2005, 120:303–313
24. Gumienny TL, Brugnera E, Tosello-Trampont AC, Kinchen JM, Haney LB, Nishiwaki K, Walk SF, Nemergut ME, Macara IG, Francis R, Schedl T, Qin Y, Van Aelst L, Hengartner MO, Ravichandran KS: CED-12/ELMO, a novel member of the CrkII/Dock180/Rac pathway, is required for phagocytosis and cell migration. Cell 2001, 107:27–41
25. Wilson EM, Oh Y, Hwa V, Rosenfeld RG: Interaction of IGF-binding protein-related protein 1 with a novel protein, neuroendocrine differentiation factor, results in neuroendocrine differentiation of prostate cancer cells. J Clin Endocr Metab 2001, 86:4504–4511
26. Chien J, Staub J, Hu SI, Erickson-Johnson MR, Couch FJ, Smith DI, Crowl RM, Kaufmann SH, Shridhar V: A candidate tumor suppressor HtrA1 is downregulated in ovarian cancer. Oncogene 2004, 23:1636–1644
27. Markowitz S, Wang J, Myeroff L, Parsons R, Sun L, Lutterbaugh J, Fan RS, Zbrowska E, Kinzler KW, Vogelstein B, Brattain M, Willson JKV: Inactivation of the type II TGF-beta receptor in colon cancer cell with microsatellite instability. Science 1995, 268:1336–1338
28. He B, You L, Uematsu K, Zang K, Xu Z, Lee AY, Costello JF, McCormick F, Jablons DM: SOCS-3 is frequently silenced by hypermethylation and suppresses cell growth in human lung cancer. Proc Natl Acad Sci USA 2003, 100:14133–14138
29. Lagos-Quintana M, Rauhut R, Yalcin A, Meyer J, Lendeckel W, Tuschl T: Identification of tissue-specific microRNAs from mouse. Curr Biol 2002, 12:735–739
30. Aravin AA, Lagos-Quintana M, Yalcin A, Zavolan M, Marks D, Snyder B, Gaasterland T, Meyer J, Tuschl T: The small RNA profile during Drosophila melanogaster development. Dev Cell 2003, 5:337–350
31. Suh MR, Lee Y, Kim JY, Kim SK, Moon SH, Lee JY, Cha KY, Chung HM, Yoon HS, Moon SY, Kim VN, Kim KS: Human embryonic stem cells express a unique set of microRNAs. Dev Biol 2004, 270:488–498
32. Barroso-del Jesus A, Romero-López C, Lucena-Aguilar G, Melen GJ, Sanchez L, Ligero G, Berzal-Herranz A, Menendez P: Embryonic stem cell-specific miR302-367 cluster: human gene structure and functional characterization of its core promoter. Mol Cell Biol 2008, 28:6609–6619
33. Sherr CD, Roberts JM: CDK inhibitors: positive and negative regulators of G1-phase progression. Genes Dev 2001, 13:1501–1512
34. Yamaguchi H, Condeelis J: Regulation of the actin cytoskeleton in cancer cell migration and invasion. Biochim Biophys Acta 2007, 1773:642–652
35. Carreira S, Goodall J, Denat L, Rodriguez M, Nuciforo P, Hoek KS, Testori A, Larue L, Goding CR: Mitf regulation of Dia1 controls melanoma proliferation and invasiveness. Genes Dev 2006, 20:3426–3439
36. Fromique O, Hamidouche Z, Marie PJ: Nlockade of the RhoA-JNK-c-Jun-MMP2 cascade by atorvastatin reduces osteosarcoma cell invasion. J Biol Chem 2008, 283:30549–30556
37. Sugimoto K, Ishibashi T, Sawamura T, Inoue N, Kamioka M, Uekita H, Ohkawara H, Sakamoto T, Sakamoto N, Okamoto Y, Takuwa Y, Kakino A, Fujita Y, Tanaka T, Teramoto T, Maruyama Y, Takeishi Y: LOX-1-MT1-MMP axis is crucial for RhoA and Rac1 activation induced by oxidized low-density lipoprotein in endothelial cells. Cardiovasc Res 2009, 84:127–136
38. Besson A, Gurian-West M, Schmidt A, Hall A, Roberts JM: p27Kip1 modulates cell migration through the regulation of RhoA activation. Genes Dev 2004, 18:862–876
39. Weinberg RA: Multistep tumorigenesis: the biology of cancer. Edited by RA Weinberg. Garland Science, New York, NY 2007, pp 399–462
40. Lee J, Kim JY, Kang IY, Kim HK, Han YM, Kim J: The EWS-Oct-4 fusion gene encodes a transforming gene. Biochem J 2007, 406:519–526
41. Boyer LA, Lee TI, Cole MF, Johnstone SE, Levine SS, Zucker JP, Guenther MG, Kumar RM, Murray HL, Jenner RG, Gifford DK, Melton DA, Jaenisch R, Young RA: Core transcriptional regulatory circuitry in human embryonic stem cells. Cell 2005, 122:947–956
42. Loh YH, Wu Q, Chew JL, Vega VB, Zhang W, Chen X, Bourque G, George J, Leong B, Liu J, Wong KY, Sung KW, Lee CW, Zhao XD, Chiu KP, Lipovich L, Kuznetsov VA, Robson P, Stanton LW, Wei CL, Ruan Y, Lim B, Ng HH: The Oct4 and Nanog transcription network regulates pluripotency in mouse embryonic stem cells. Nat Genet 2006, 38:431–440
43. Greer Card DA, Hebbar PB, Li L, Trotter KW, Komatsu Y, Mishina Y, Archer TK: Oct4/Sox2-regulated miR-302 targets cyclin D1 in human embryonic stem cells. Mol Cell Biol 2008, 28:6426–6438

Clin Exp Metastasis (2010) 27:389–397
DOI 10.1007/s10585-010-9313-4

RESEARCH PAPER

Lung cancer progression and metastasis from the prognostic point of view

Kentaro Inamura · Yuichi Ishikawa

Received: 7 March 2009 / Accepted: 16 February 2010 / Published online: 12 March 2010
© Springer Science+Business Media B.V. 2010

Abstract Lung cancer is the leading cause of cancer death in men and women worldwide. Since the occurrence of metastases in distant organs is the major reason for mortality of cancer patients, we need to elucidate the underlying mechanisms. Many studies featuring analysis of gene expression, comparative genomic hybridization and loss of heterozygosity analysis have been performed and generated support for the hypothesis that metastatic potential is acquired early in tumorigenesis. Furthermore, it is now clear that the majority of tumor cells have the potential to metastasize. Although many changes in gene expression profiles have been established retrospectively, translational research is now a high priority to enable clinical application and treatment based on laboratory findings.

Keywords Lung cancer · Metastasis · Prognosis · Gene expression · Comparative genomic hybridization · Loss of heterozygosity analysis

Introduction

Lung cancer, the leading cause of cancer death in men and women worldwide and continuing to rise in frequency, is generally classified as of either small-cell lung carcinoma (SCLC) or non-SCLC (NSCLC) types. Within these groups further distinctions are made, with NSCLCs sub-divided into adenocarcinomas, squamous cell carcinomas (SCCs), and large cell carcinomas (LCCs). The occurrence of metastases in distant organs is the major cause of death for the vast majority of lung cancer patients. Clinical outcomes can be roughly predicted by pathological-Stage (p-Stage) and 5 year survival for p-Stage I cases, pathologically lacking metastases, is relatively good, ranging from 60 [1] to 90% [2]. Even when cancer lesions have been fully removed and no metastasis is found at surgery, however, some patients with p-Stage I lesions suffer recurrence and die of cancer relapse. Presumably, these already had micrometastases at the time of tumor removal. To avoid unnecessary lymph node dissection in low-risk cases but ensure that postoperative adjuvant therapy is performed for high-risk patients, we need a clinically useful approach to better stratify patients with respect to the risk of recurrence. Towards a rational treatment, we need to elucidate metastatic gene signatures and molecular mechanisms of lung cancer progression. The aim of the present review is to survey findings on lung cancer progression and metastasis from the prognostic point of view, especially emphasizing our study [3] paying attention to heterogeneity of lung cancers, an important characteristic.

The beginning of gene expression profiling in lung cancers

In November, 2001, pioneering studies of gene expression profiling in lung cancers were reported at the same time by a Stanford University group [4] and a Harvard University group [5]. Subdivision of the tumors based on gene expression faithfully recapitulated their histological classification and characteristic expression profiles for each histological type could be identified. The insulinoma-associated gene 1 (IA-1) and the human achaetescute homolog 1 (hASH1) were found to be neuroendocrine SCLC markers, shared also

K. Inamura · Y. Ishikawa (✉)
Department of Pathology, The Cancer Institute, Japanese Foundation for Cancer Research (JFCR), 3-10-6 Ariake, 135-8550 Koto-ku, Tokyo, Japan
e-mail: ishikawa@jfcr.or.jp

by carcinoid tumors. Identified as SCC markers were Keratin 5 (KRT5), KRT17 and Tumor protein p63, which is associated with development of squamous epithelium. Supporting the traditional view that lung adenocarcinomas are a heterogeneous group, distinct subclasses were evident. One adenocarcinoma subgroup was comprised of tumors expressing neuroendocrine markers, such as hASH1 and IA-1, associated with a significant decrease in patient survival when compared to other adenocarcinomas [5]. Another subgroup appeared to express markers of alveolar type II pneumocytes and was characterized by high relative expression of TTF1 or surfactant protein genes.

Gene expression profiling predicting survival of patients with lung adenocarcinomas

As mentioned above, the Stanford University group [4] and the Harvard University group [5] first identified prognostically different subgroups of adenocarcinomas by gene expression profiling. One subgroup with a poor prognosis was revealed to have neuroendocrine features. Subsequently, many further studies using gene expression profiling have been reported. Beer et al. [6] described development of a risk index, compiling the relative expression of 50 genes, to identify high or low risk groups of Stage I adenocarcinomas that correlated with patient survival.

Ramaswamy et al. [7] compared gene expression profiles of adenocarcinoma metastases and unmatched primary adenocarcinomas and found patterns that allowed distinction between the two, but also reported that a subset of primary tumors had similar expression to metastases. This finding led them to challenge "the notion that metastases arise from rare cells within the primary tumor." They suggested that the majority of tumor cells have the potential to metastasize, but this remains controversial and Liotta and Kohn have argued against their conclusions [8]. When lists of genes are examined, it is unclear whether the expression profile is a cause or a local consequence of the metastatic process. Ramaswamy et al. did not microdissect tumor cells for analysis of their tissue specimens and consequently the gene-expression pattern data reflect contributions from multiple cell populations. Thus, the expression pattern of the genes in the authors' signature set may be at least partially due to activated host stromal elements. Indeed, two of the important upregulated genes in the list encode stromal collagen.

Although gene expression profiles that can classify cancer patients according to the risk of recurrence have been found, most studies have been retrospective. Very recently, Potti et al. [9] documented a "lung metagene model" that can identify individuals at increased risk for disease recurrence with stage IA NSCLC, which they now plan to use for a prospective randomized clinical trial. Translational research is now an urgent priority to enable clinical application of basic research findings.

Gene expression profiling using hierarchical clustering and non-negative matrix factorization in squamous cell carcinomas

After the adenocarcinoma, the SCC is the most frequent lung cancer histology, accounting for approximately 30% of the total. Its development is the most strongly related to smoking. For adenocarcinomas, subclassification by differentiation grade [10] or histological pattern [2] is useful to predict prognosis. For SCCs, differentiation grade is used for pathological subclassification, but it correlates poorly with prognosis. Although SCCs demonstrate some histological variation, such as with the basaloid variant, this does not allow good prediction of prognosis. The present system used to subclassify SCC is thus insufficient and we have therefore attempted to make a clinically useful classification based on gene expression profiling [11]. By hierarchial clustering, we subclassified SCCs into two prognostically significant subclasses. Furthermore, consensus clustering with a non-negative matrix factorization (NMF) approach indicated the robustness of this classification (Fig. 1). NMF appears to be more accurate for choice of input genes than hierarchial clustering and can be combined with a quantitative evaluation of the robustness with numbers of clusters [12]. Both hierarchical clustering and NMF approaches (Fig. 1) indicated that SCCs can be divided into two groups, SCC-A and SCC-B, with prognostic variation (Fig. 2a). The cophenetic correlation coefficient, k, quantitatively indicated the two-centroid clustering to be the most robust with the highest value, as attested by clear block diagonal patterns (Fig. 2b). Up-regulation of cell-proliferation-related genes was evident in the subclass with poor survival. In the subclass with better survival, genes involved in differentiated intracellular functions, such as the MAPKKK cascade, ceramide metabolism, or regulation of transcription, were upregulated.

Histological typing and gene expression profiles in high-grade neuroendocrine tumors

The current WHO classification of high-grade neuroendocrine tumors (HGNTs) currently recognizes large-cell neuroendocrine carcinoma (LCNEC), a subclass of LCC, and SCLC as a distinct group [13]. Since LCNEC and SCLC share several histological features, a consensus differential diagnosis between LCNEC and SCLC is sometimes difficult, even among experienced lung pathologists. Hence, by the microarray technique, we analyzed gene

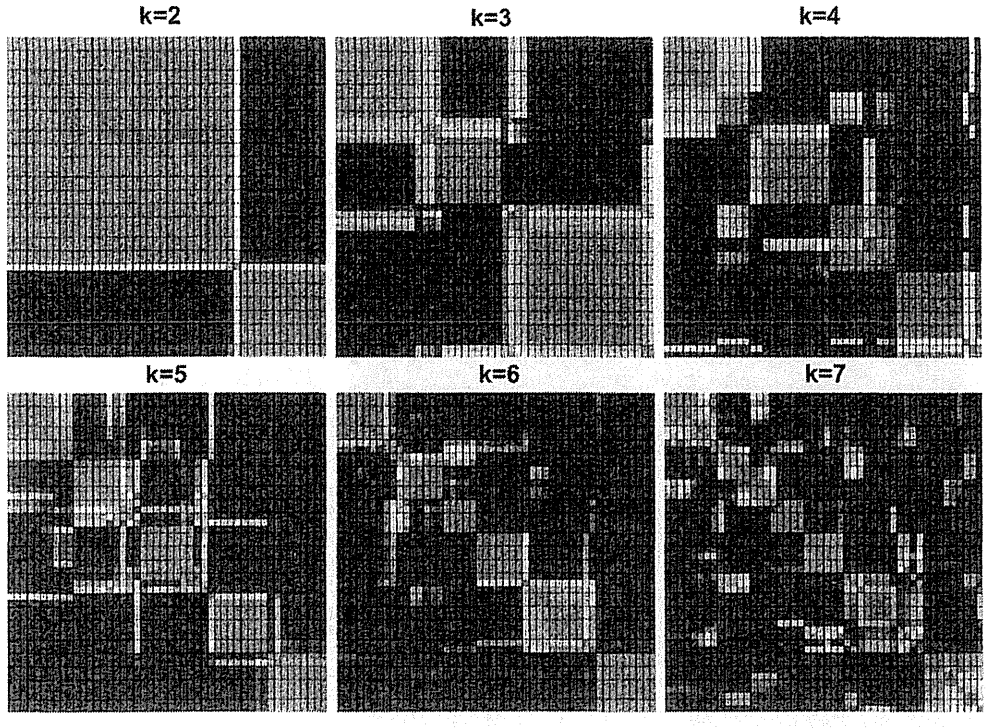

Fig. 1 Reordered consensus averaging 50 connectivity matrices computed at $k = 2$–7 for all SCC samples with 3,344 genes. Samples were hierarchically clustered, colored from 0 (samples never in the same cluster) to 1 (samples always in the same cluster)

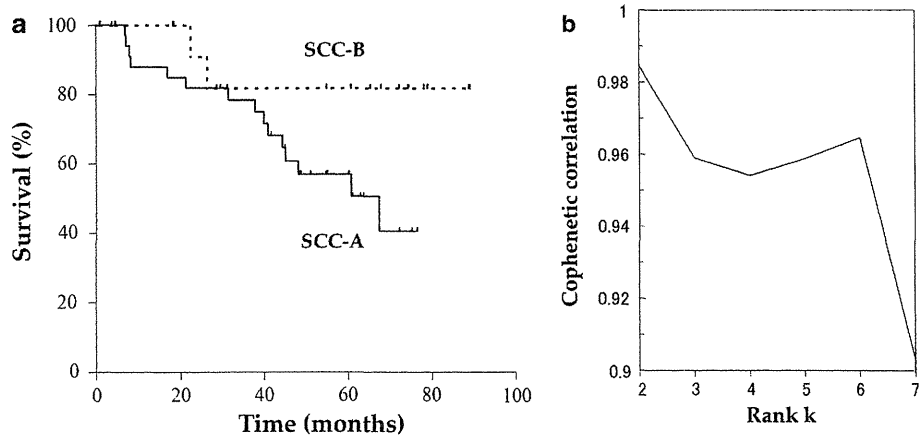

Fig. 2 **a** Kaplan–Meier survival curves for the 48 SCC patients (SCC-A vs. SCC-B). **b** Cophenetic correlation coefficients for the hierarchically clustered matrices

expression profiles of HGNTs with other histological tumor groups and normal lung tissue [14]. By hierarchical clustering, we could readily identify distinct groups for carcinoids, LCC, adenocarcinoma, and normal lung (Fig. 3a). While we could not subclassify SCLC and LCNEC by gene expression profiling, two prognostically significant subtypes of HGNT were evident, independent of SCLC and LCNEC ($P = 0.0094$). Many genes distinguished the HGNT groups. There was no significant difference in survival between SCLC and LCNEC samples (Fig. 3b; $P = 0.37$).

Integrated classification of lung tumors and cell lines by expression profiling

The utility of cancer cell lines depends largely on their accurate classification, commonly based on histopathological diagnosis of the cancers from whom they were derived. However, because cancers are often heterogeneous, cell lines, which also have a propensity to alter in vitro, may not be truly representative. We therefore performed gene expression profiling, which can faithfully recapitulate histological classification of tumors, to examine different cell